NASA Contractor Report 178182

(NASA-CR-178182) GUIDANCE LAW SIMULATION STUDIES FOR COMPLEX APPROACHES USING THE MICROWAVE LANDING SYSTEM (MLS) (Douglas Aircraft Co., Inc.) 80 p CSCL 17G

N87-12552

Unclas

G3/04 44660

Guidance Law Simulation Studies for Complex Approaches Using the Microwave Landing System (MLS)

J. B. Feather

McDonnell Douglas Corporation
Douglas Aircraft Company
Long Beach, California 90846

Contract NAS1-18028
November 1986

National Aeronautics and
Space Administration

Langley Research Center
Hampton, Virginia 23665

NASA Contractor Report 178182

Guidance Law Simulation Studies for Complex Approaches Using the Microwave Landing System (MLS)

J. B. Feather

McDonnell Douglas Corporation
Douglas Aircraft Company
Long Beach, California 90846

Contract NAS1-18028
November 1986

National Aeronautics and
Space Administration

Langley Research Center
Hampton, Virginia 23665

TABLE OF CONTENTS

	PAGE
LIST OF FIGURES	iii
LIST OF TABLES	vi
LIST OF SYMBOLS	vii
SUMMARY AND INTRODUCTION	1
CONCLUSIONS AND RECOMMENDATIONS	2
MLS OPERATIONS	3
COVERAGE VOLUME	3
APPROACH GEOMETRY	4
APPROACH PATH DESCRIPTIONS	5
WASHINGTON NATIONAL RIVER APPROACH	5
GUIDANCE CONCEPTS	6
WAYPOINT TRANSFORMATION	6
LATERAL GUIDANCE EQUATIONS	7
Along-Track Distance Computations	7
Lateral Complementary Filters	9
Linear Leg Steering Commands	10
Turn Anticipation	11
Circular Leg Steering Commands	11
Turn Termination	12
VERTICAL GUIDANCE EQUATIONS	13
SPEED CONTROL	15
SIMULATION DESCRIPTION	16
MD-80 SIMULATION PROGRAM	16
WIND AND TURBULANCE MODELS	16

TABLE OF CONTENTS (Con't)

	PAGE
WINDSHEAR	17
MLS NOISE MODELS	17
SIMULATION RESULTS	19
ENTRY APPROACH RESULTS	19
Case 1.	19
Case 2.	20
Case 3.	20
Case 4.	21
TERMINAL AREA APPROACH RESULTS	21
Case 5.	22
Case 6.	22
Case 7.	23
Case 8.	23
Case 9.	23
Case 10.	23
FIXED BASE SIMULATOR CONSIDERATIONS	24
REFERENCES	25

LIST OF FIGURES

		PAGE
1.	Existing ILS Coverage	34
2.	Extended Coverage Possible with MLS	35
3.	MLS Approach Geometry	36
4.	Waypoints for Washington National River Approach	36
5.	Waypoint Transformation Geometry	37
6.	Lateral Guidance Geometry	37
7.	Lateral Guidance Flow Diagram (Sheets 1 and 2)	38-39
8.	Lateral Tracking Error for Linear Leg	40
9.	Turn Anticipation Geometry	40
10.	Lateral Tracking Error for Circular Leg	41
11.	Turn Termination Geometry	41
12.	Vertical Tracking Error for First Glideslope	42
13.	Vertical Tracking Error for Second Glideslope	42
14.	Block Diagram of the Vertical Steering Algorithm	43
15.	Vertical Guidance Flow Diagram (Sheets 1 and 2)	44-45
16.	Block Diagram of MLS Pitch and Roll Guidance Systems	46
17.	Turbulence Model Used in Simulation	46
18.	MLS Noise Model as Used in Simulation (1σ or 68% Probability)	46
19.	Bank Angle, Case 1 (Initial Approach, Baseline)	47
20.	Pitch Angle, Case 1 (Initial Approach, Baseline)	47
21.	Lateral Tracking Error, Case 1 (Initial Approach, Baseline)	48
22.	Vertical Tracking Error, Case 1 (Initial Approach, Baseline)	48
23.	Vertical Speed, Case 1 (Initial Approach, Baseline)	49
24.	Ground Track, Case 1 (Initial Approach, Baseline)	49

LIST OF FIGURES (Con't)

		PAGE
25.	Bank Angle, Case 2 (Initial Approach, MLS Noise)	50
26.	Lateral Tracking Error, Case 2 (Initial Approach, MLS Noise) . .	50
27.	Pitch Angle, Case 2 (Initial Approach, MLS Noise)	51
28.	Vertical Tracking Error, Case 2 (Initial Approach, MLS Noise) .	51
29.	Vertical Speed, Case 2 (Initial Approach, MLS Noise)	52
30.	Bank Angle, Case 3 (Initial Approach, Wind)	52
31.	Lateral Tracking Error, Case 3 (Initial Approach, Wind)	53
32.	Bank Angle, Case 4 (Initial Approach, Speed Change)	53
33.	Lateral Tracking Error, Case 4 (Initial Approach, Speed Change)	54
34.	Airspeed, Case 4 (Initial Approach, Speed Change)	54
35.	Bank Angle, Case 5 (Final Approach, Baseline)	55
36.	Pitch Angle, Case 5 (Final Approach, Baseline)	55
37.	Lateral Tracking Error, Case 5 (Final Approach, Baseline). . . .	56
38.	Vertical Tracking Error, Case 5 (Final Approach, Baseline). . .	56
39.	Vertical Speed, Case 5 (Final Approach, Baseline)	57
40.	Ground Track, Case 5 (Final Approach, Baseline)	57
41.	Bank Angle, Case 6 (Final Approach, MLS Noise)	58
42.	Lateral Tracking Error, Case 6 (Final Approach, MLS Noise). . .	58
43.	Pitch Angle, Case 6 (Final Approach, MLS Noise)	59
44.	Vertical Tracking Error, Case 6 (Final Approach, MLS Noise). . .	59
45.	Vertical Speed, Case 6 (Final Approach, MLS Noise)	60
46(A).	Lateral Tracking Error, Case 7 (Final Approach, Wind)	61
46(B).	Lateral Tracking Error, Case 8 (Final Approach, Turbulence) . .	61
47(A).	Vertical Tracking Error, Case 7 (Final Approach, Wind)	62
47(B).	Vertical Tracking Error, Case 8 (Final Approach, Turbulence) . .	62

LIST OF FIGURES (Con't)

		PAGE
48.	Ground Track, Case 8 (Final Approach, Turbulence)	63
49.	Bank Angle, Case 9 (Final Approach, Windshear)	63
50.	Lateral Tracking Error, Case 9 (Final Approach, Windshear) . . .	64
51.	Vertical Tracking Error, Case 9 (Final Approach, Windshear) . .	64
52.	Lateral Tracking Error, Case 10 (Final Approach, Light Weight).	65
53.	Interfaces between MLS Guidance Computer and Existing Aircraft Systems	66

LIST OF TABLES

		PAGE
1.	Washington National River Waypoints	26
2.	Transformed River Waypoints	27
3.	Values for Simulated Windshear	28
4.	MLS Noise Models (2σ or 95% Probability)	29
5.	Simulated Case Configurations	30
6.	Tracking Errors at 100 FT Decision Height	31
7.	Lateral Guidance Signal Computation Diagram	32
8.	Vertical Guidance Signal Computation Diagram	33

LIST OF SYMBOLS

A	Angle defining the arc length of a turn, rad.
A_1, A_2, A_3	Angles associated with three adjacent waypoints, rad.
C	Distance from aircraft position to last waypoint, ft.
C_1, C_2, C_3	Difference equation coefficients for the vertical complementary filter, ND
C_T	Total chord length between two adjacent waypoints, ft.
D	Distance from aircraft position to last waypoint, ft.
D_A	Distance used to determine when to start turn anticipation, ft.
D_C	Total distance along circular arc between two adjacent waypoints, ft.
D_I	Distance along desired path from aircraft position to last waypoint, ft.
D_L	Leg distance between two adjacent waypoints for a linear leg, ft.
D_{LG}	Leg distance (linear or circular), ft.
D_S	Distance to next waypoint, ft.
D_{TG}	Distance to go to origin, measured in ground plane, ft.
d	Distance from AZ/DME transmitter to coordinate origin, ft.
$G_{L_1}, G_{L_2}, G_{L_3}, G_{L_4}$	Guidance system gains for lateral steering commands
G_S	Glideslope angle for current leg, deg
$G_{V_2}, G_{V_3}, G_{V_4}$	Guidance system gains for vertical steering commands
h	Altitude, ft.
Δh	Altitude deviation from desired value, ft.
$\Delta \hat{h}$	Computed vertical tracking error signal, ft.
$\Delta \hat{\dot{h}}$	Computed vertical tracking error rate signal, ft./sec.

$\hat{\ddot{h}}$	Vertical acceleration, ft./sec.^{2}
h_D	Desired altitude to glideslope for current leg, ft.
$\dot{h}_F$	Filtered altitude rate, ft./sec.
h_m	Altitude derived from MLS angles and range signals, ft.
I_R	Integer defining left or right turn, ND
i_S	Integer that defines a three-waypoint set, ND
ℓ_1, ℓ_2	Distances from MLS antenna to CG, ft.
R	Radius of circular turn, ft.
ΔR	Computed lateral tracking error during circular turn, ft.
$\Delta\dot{R}$	Computed lateral tracking error rate during circular turn, ft./sec.
R_{DME}	Range from DME/P transmitter to MLS aircraft antenna, ft.
S_x, S_y, S_z	Wind magnitude at 33 ft. altitude in earth coordinates, KT
T_{DTG}	Total distance to go measured along desired path in the ground plane, ft.
ΔT	Digital computer simulation integration interval, sec.
u_g, v_g, w_g	Turbulence levels along x-y-z axes, KT
V_G	Ground speed, ft./sec.
W	Wind factor as a function of altitude, ND
WP	Waypoint identifier, ND
W_X, W_Y, W_Z	Wind magnitudes at altitude h in earth coordinates, KT
W_{TX}, W_{TY}, W_{TZ}	Total winds (including turbulence), KT
x,y,h	Coordinates of a given waypoint, ft.
x_C, y_C	Coordinates of the center of the turn circle, ft.
x'_m, y'_m, z'_m	Coordinates defining MLS antenna location, ft.

LIST OF SYMBOLS (Cont'd)

$\hat{x}'_m, \hat{y}'_m, \hat{z}'_m$	Filtered signals defining MLS antenna location, ft.
$\hat{x}_m, \hat{y}_m, \hat{z}_m$	Filtered signals defining CG location, ft.
$\hat{\dot{x}}_m, \hat{\dot{y}}_m$	Filtered rate signals for CG location, ft./sec.
$\ddot{x}, \ddot{y}$	Accelerations used in lateral complementary filter, ft./sec.^{2}
Δy	Computed lateral tracking error signal during linear leg, ft.
$\Delta \dot{y}$	Computed lateral track error rate during circular leg, ft./sec.
Δz_1	Component of computed vertical tracking error rate derived from vertical acceleration, ft./sec.
Δz_2	Component of computed vertical tracking error rate drived from vertical tracking error, ft./sec.
γ	Vertical flight path angle, deg.
$\Delta\psi$	Course angle error, deg.
$\varepsilon_x, \varepsilon_y$	Error signals used in lateral complementary filter, ft.
$\dot{\varepsilon}_x, \dot{\varepsilon}_y$	Rate error signals used in lateral complementary filter, ft./sec.
θ	Aircraft pitch angle, deg.
θ_{AZ}	MLS azimuth angle, deg.
θ_{CI}	Integral component of pitch steering command, deg.
θ_{CE}	Pitch steering command, deg.
θ_{EL}	MLS elevation angle, deg.
θ_P	Pitch predict angle, deg.
θ_{STR}	Pitch steering signal, deg.
τ	Time constant, sec.
ϕ	Bank angle, deg.
ϕ_{STR}	Bank steering command, deg.

ψ_D	Desired course angle, deg.
ψ_G	Ground track angle, deg.
ψ_R	Reference course angle, deg.

SUMMARY AND INTRODUCTION

This report contains results of a follow-on effort on the NASA Advanced Transport Operating Systems (ATOPS) Technology Studies contract (NAS1-16202). This previous task, sponsored jointly by NASA and the FAA, was a study of curved, descending approaches using the microwave landing system (Ref. 1). The major goal of the present study is to generalize the lateral and vertical guidance algorithms to be applicable to any desired approach path defined by waypoints specified in a general form, rather than being restricted to the particular approach paths previously studied.

Waypoint data for the Washington National river approach was used with the generalized guidance laws in an MD-80 simulation program. Results from this program consist of performance data, which included lateral and vertical tracking errors, bank and pitch angle time histories, and ground track trajectories. The river approach was defined by seven waypoints and contained a pitchover to a 3 deg glideslope during the first turn.

Ten cases were simulated for the river approach. Four cases started at entry to the approach and included two turns and the pitchover. These cases were run to study the effects of MLS noise, steady winds, and a speed change. The remaining six cases contained four turns at a constant glideslope down to 100 feet altitude. These runs provided data on the effects of MLS noise, steady winds, turbulence, windshear, and a light-weight configuration.

CONCLUSIONS AND RECOMMENDATIONS

The goals of the present study (to generalize previously developed guidance algorithms and to generate performance data for a particular simulated approach) have been achieved. A generalized waypoint database was established and a method developed that allowed almost any approach path to be specified. It became necessary to completely reformulate the lateral guidance algorithm to accommodate this new path definition concept. Only minor changes to the vertical algorithm were required. These revised guidance laws do work well with this new path definition. Tracking errors for ten different cases were generated and were within acceptable limits.

There are two major areas that have been identified for potential follow-on tasks. They are missed approach/precision departures and fixed-base simulator evaluations. For the departure studies, the following specific tasks are recommended:

- Develop path definition for departures using only the back azimuth angle and range information.

- Establish lateral and vertical guidance algorithms that can be used with both missed approaches and precision departures.

- Simulate the missed approach/precision departures and evaluate system tracking performance.

For the simulator evaluations, preliminary analytical efforts indicated the following tasks:

- Formulate studies to establish system architecture with regard to a fixed-base simulator.

- Coordinate MLS/guidance computer hardware/software interfaces.

- Develop a guidance computer in connection with real time simulator implementation.

MLS OPERATIONS

Basically, the MLS consists of ground stations, an airborne receiver, and a display/control panel for the pilot. A type of operation, called an ILS "look-alike", is where conventional approaches would be flown using the MLS equipment. Initially, existing aircraft can be reconfigured to operate in this mode since it requires minimum airborne equipment changes. To realize the additional benefits of MLS over ILS, an on-board guidance computer is added to process steering signals for complex, curved paths. A database of waypoints (distances, altitudes, speeds) is also required as part of the system. The guidance computer uses the MLS signals and waypoint data to generate steering commands for landing and departures. These commands can be used to drive a flight director for pilot-in-the-loop operation. Alternately, the signals can drive the autopilot directly to provide autoflight operation. This latter mode is the one for which performance data were generated in the present study.

COVERAGE VOLUME

Figure 1 is a sketch of the existing ILS coverage characterized by its narrow beam. Signals for landing (provided by localizer and glideslope transmitters) are available only within the indicated volume. In contrast, Figure 2 represents the MLS coverage showing the possibility of curved paths, segmented glideslope, path lengthening,as well as ILS look-alike approaches. This coverage is provided by an azimuth transmitter (AZ), an elevation transmitter (EL), and precision distance measuring equipment (DME/P). Both the AZ and EL antennas radiate scanned beams to provide angular coverage in the indicated volume. The DME/P (colocated with the AZ equipment) is omnidirectional and provides precision range information to the aircraft.

Also shown in Figure 2 is the coverage for takeoff and go around. This coverage is provided by a back AZ antenna and the same DME/P as used for landing. Elevation angle information is not available for takeoff or go around.

APPROACH GEOMETRY

Angle and range variables for landing are defined in Figure 3. The AZ-DME/P equipment is located 1000 feet from the end of the runway (a 10,000 feet runway was assumed for this study). The EL transmitter is actually located 400 feet from the runway centerline, but to simplify the simulation it was assumed to be at the coordinate origin.

The position of the aircraft MLS antenna relative to the ground equipment can be calculated from θ_{AZ} , θ_{EL} , and R_{DME}. For the assumed rectangular coordinate system, the following equations result:

$$y_m' = -R_{DME} \sin \theta_{AZ} \tag{1}$$

$$x_m' = d \cos^2 \theta_{EL} - \left[\cos^2 \theta_{EL}(R_{DME}^2 - d^2 \sin^2 \theta_{EL}) - y_m'^2\right]^{\frac{1}{2}} \tag{2}$$

$$z_m' = - \left[x_m'^2 + y_m'^2\right]^{\frac{1}{2}} \tan \theta_{EL} \tag{3}$$

In Eqn(2), the term d is the distance from the ground coordinate center to the AZ/DME location. Altitude to the CG is positive for the geometry shown, so $h_m'=-z_m'$. In a later section, these position coordinates will be corrected for the offset of the aircraft MLS antenna from the CG.

APPROACH PATH DESCRIPTIONS

WASHINGTON NATIONAL RIVER APPROACH

Six waypoints, and the glide slope intercept point, were defined for the Washington National river approach. These waypoints are identified by name in Figure 4. One additional waypoint was added so the first part of the simulated flight would be at a constant altitude. Pitch over to a 3 deg glideslope is specified at ENTRY. Coordinates for the waypoints are given in Table 1. The radii shown were used in the simulation, although other values could be chosen for the same waypoint sequence.

The numbered waypoints in Figure 4 are the points of turn entry and turn exit computed by the algorithms for circular transitions. Waypoint 1 was selected at an altitude of 100 feet, waypoints 2 and 3 define the end and beginning of the turn at FAF18, etc. Waypoint 14 was arbitrarily selected as the starting point for the simulated runs. These 14 waypoints are used by the lateral and vertical guidance laws to define the desired approach path. The definition of these waypoints and their numerical values will be discussed in a later section.

GUIDANCE CONCEPTS

Although the present study uses the same basic MD-80 simulation program as reported in Reference 1, the lateral and vertical subroutines were completely rewritten. This revision was due to the generalization of the previous lateral and vertical guidance laws. A maximum of 20 waypoints can now be accommodated and the approach can be simulated. Flow charts and equations for these guidance concepts are discussed in detail in the following sections.

WAYPOINT TRANSFORMATION

Consider waypoints that are defined as the end points of straight-line segments or legs. If a radius is chosen for the circular part of the transition between waypoints, then the beginning and end of the turn (for a constant speed approach) are defined. These two points are uniquely determined by knowing three adjacent waypoints. Figure 5 depicts a general three-point geometry. The coordinates shown are in the ground plane, where an x-y coordinate pair is defined for each waypoint. The numbering of waypoints was chosen in decreasing order as the approach progresses. Waypoints $WP(i_s)$, $WP'(i_s-1)$, and $WP'(i_s-2)$ are the three input points. The integer i_s identifies the particular set of points and is used in the transformation calculations. The points $WP(i_s-1)$ and $WP(i_s-2)$ are the ones to be determined. Three angles A_1, A_2, and A_3 of Figure 5 are easily determined from the input points.

$$\left.\begin{aligned} A_1 &= \tan^{-1} \frac{y'(i_S-1) - y(i_S)}{x'(i_S-1) - x(i_S)} \quad \text{rad} \\ A_2 &= \tan^{-1} \frac{y'(i_S-2) - y(i_S-1)}{x'(i_S-2) - x(i_S-1)} \quad \text{rad} \end{aligned}\right\} \quad (4)$$

$$A_3 = \pi + I_R(i_S-1)\,(A_1-A_2) \quad \text{rad} \qquad (5)$$

where: $I_R(i_S-1) = +1$ for a right hand turn
$= -1$ for a left hand turn

The desired points on the circular arc that are tangent to the adjacent legs are calculated from:

$$x(i_S-1) = x'(i_S-1) - R(i_S-1) \cos A_1/\tan (A_3/2) \tag{6}$$

$$y(i_S-1) = y'(i_S-1) - R(i_S-1) \sin A_1/\tan (A_3/2) \tag{7}$$

$$x(i_S-2) = x'(i_S-1) + R(i_S-1) \cos A_2/\tan (A_3/2) \tag{8}$$

$$y(i_S-2) = y'(i_S-1) + R(i_S-1) \sin A_2/\tan (A_3/2) \tag{9}$$

The above process is repeated for each set of three adjacent waypoints until the transformation is complete. Results for the river approach are shown in Table 2. Once the coordinates in the x-y plane are known, the length of each leg is calculated. Altitudes at each waypoint are computed by plotting altitude vs the length of each leg. For the river approach, this plot is simply a continuous line at the 3 deg glideslope. Altitudes shown in Table 2 were computed in this manner.

LATERAL GUIDANCE EQUATIONS

The lateral guidance geometry was established by assuming the approach sequence contained a linear leg followed by a circular leg. A general two-leg segment is shown in Figure 6. Each leg is identified by the waypoint designation. Leg i_s lies between WP(i_s) and WP(i_s-1). The integer i_s starts at its maximum value (14 for the river approach) and is decreased by 2 until i_s=2. Legs 2 and 1 are both straight-line segments (between WP(2) and GPI18 in Figure 4). The flow chart in Figure 7 shows the general program flow for the lateral guidance subroutine. Reference is made to the equations that are programmed in the subroutine as explained in the following sections.

Along-Track Distance Computations.

Each leg distance is computed by the lateral guidance subroutine, which also calculates the distance to go along the curved path (measured in the x-y plane). This distance is computed as a function of time. Centers of the circular arcs are also computed for use in the roll steering command.

First, the desired course angle, $\psi_D\ (i_s)$, is calculated:

$$\psi_D(i_S) = \tan^{-1} \frac{y(i_S-1) - y(i_S)}{x(i_S-1) - x(i_S)} \quad \text{rad} \tag{10}$$

where $0 \leq \psi_D(i_S) < 2\pi$

Next, the linear leg distance is computed, followed by the total chord length for the entire circular leg. The arc length for the circular leg is computed from this chord length:

$$D_L(i_S) = \left[\left(x(i_S-1) - x(i_S)\right)^2 + \left(y(i_S-1) - y(i_S)\right)^2 \right]^{\frac{1}{2}} \tag{11}$$

$$C_T(i_S-1) = \left[\left(x(i_S-2) - x(i_S-1)\right)^2 + \left(y(i_S-2) - y(i_S-1)\right)^2 \right]^{\frac{1}{2}} \tag{12}$$

$$D_C(i_S-1) = 2R(i_S-1) \sin^{-1}\left(\frac{.5C_T(i_S-1)}{R(i_S-1)} \right) \tag{13}$$

Arc center for the curve starting at $WP(i_s-1)$ is found from:

$$x_C(i_S-1) = x(i_S-1) - I_R(i_S-1)\ R(i_S-1) \sin \psi_D(i_S) \tag{14}$$

$$y_C(i_S-1) = y(i_S-1) + I_R(i_S-1)\ R(i_S-1) \cos \psi_D(i_S) \tag{15}$$

Leg distances for legs i_s and i_s-1 (including i_s=2) are computed from:

$$D_{LG}(i_S) = D_L(i_S) \tag{16}$$

$$D_{LG}(i_S-1) = D_C(i_S-1) \tag{17}$$

Total distance to go is found by summing each leg distance for $i_s < 2$.

$$T'_{D_{TG}} = \sum_{i_S} \left[D_L(i_S) + D_C(i_S-1) \right] \qquad (i_S < 2)$$

The final two linear leg distances are added in separately.

$$D_C(1) = \left[x(1)^2 + y(1)^2 \right]^{\frac{1}{2}}$$

$$D_{LG}(2) = D_L(2) \qquad\qquad (i_S = 2)$$

$$D_{LG}(1) = D_C(1)$$

$$T_{D_{TG}} = T'_{D_{TG}} + D_L(2) + D_C(1) \tag{18}$$

A quantity, D_1, that will be used in computing the distance to go as a function of time is initialized at this point, and D_{TG} is initially set to $T_{D_{TG}}$:

$$D_1 = T_{D_{TG}} \tag{19}$$

$$D_{TG} = T_{D_{TG}} \tag{20}$$

Lateral Complementary Filter.

Lateral position coordinates from the MLS, equations (1) and (2), are processed using complementary filters. These filters are the same as those used in Reference 1. For completeness, the equations for the filtered position coordinates ($\hat{x}'_m, \hat{y}'_m$) and the filtered rate coordinates ($\hat{\dot{x}}_m, \hat{\dot{y}}_m$) are repeated below:

$$\varepsilon_x = x'_m - \hat{x}'_m \qquad |\varepsilon_x| \leq 500 \text{ ft}$$

$$\varepsilon_y = y'_m - \hat{y}'_m \qquad |\varepsilon_y| \leq 500 \text{ ft}$$

$$\varepsilon_{\dot{x}} = \frac{1}{\Delta T}\left[x'_m - x'_{m-}\right] - \hat{\dot{x}}_{m-}$$

$$\varepsilon_{\dot{y}} = \frac{1}{\Delta T}\left[y'_m - y'_{m-}\right] - \hat{\dot{y}}_{m-}$$

$$\hat{x}'_m = \hat{x}'_{m-} + \Delta T\left[0.654\varepsilon_x + \hat{\dot{x}}_{m-}\right] \tag{21}$$

$$\hat{y}'_m = \hat{y}'_{m-} + \Delta T\left[0.654\varepsilon_y + \hat{\dot{y}}_{m-}\right] \tag{22}$$

$$\hat{\dot{x}}_m = \hat{\dot{x}}_{m-} + \Delta T\left[0.129\varepsilon_x + 0.125\varepsilon_{\dot{x}} + \ddot{x}\right] \tag{23}$$

$$\hat{\dot{y}}_m = \hat{\dot{y}}_{m-} + \Delta T\left[0.129\varepsilon_y + 0.125\varepsilon_{\dot{y}} + \ddot{y}\right] \tag{24}$$

In the above equations, the minus subscript denotes the first past value of the variable.

The ground track angle, ψ_G , is computed from the rate estimates. The position estimates are corrected for the MLS antenna being displaced ℓ_1 feet from the aircraft CG longitudinally and ℓ_2 feet vertically:

$$\psi_G = \tan^{-1}(\hat{\dot{y}}_m/\hat{\dot{x}}_m) \qquad 0 < \psi_G \leq 360° \tag{25}$$

$$\hat{x}_m = \hat{x}'_m - \ell_1 \cos \psi_G \tag{26}$$

$$\hat{y}_m = \hat{y}'_m - \ell_1 \sin \psi_G \tag{27}$$

$$\hat{h}_m = h'_m - \ell_1 \sin \theta + \ell_2 \cos \theta \tag{28}$$

Ground speed and the distance to the next waypoint are calculated from:

$$V_G = \left[\hat{\dot{x}}_m^2 + \hat{\dot{y}}_m^2 \right]^{\frac{1}{2}} \tag{29}$$

$$D_S = \left[\left(\hat{x}_m - x(i_S-1) \right)^2 + \left(\hat{y}_m - y(i_S-1) \right)^2 \right]^{\frac{1}{2}} \tag{30}$$

Linear Leg Steering Commands.

Path deviation normal to the linear leg is calculated, and this error signal is used in forming the roll steering command. In Figure 8, the aircraft position ($\hat{x}_m, \hat{y}_m$) is shown with a tracking error Δy . The following equations define the roll steering command, ϕ_{STR} , used to maintain track along the linear leg.

$$D^2 = \left[\hat{x}_m - x(i_S) \right]^2 + \left[\hat{y}_m - y(i_S) \right]^2$$

$$\Delta y = \left[\hat{y}_m - y(i_S-1) \right] \cos \Psi_D(i_S-1) - \left[\hat{x}_m - x(i_S-1) \right] \sin \psi_D(i_S-1) \tag{31}$$

$$D_I = \left[D^2 - \Delta y^2 \right]^{\frac{1}{2}} \tag{32}$$

$$\Delta\psi = \psi_G - \psi_D(i_S)$$

$$\Delta\dot{y} = V_G \sin \Delta\psi \cdot \tag{33}$$

$$\phi_{STR} = -G_{L1}(\Delta y + G_{L2}\Delta\dot{y}) \tag{34}$$

where $G_{L1} = 0.0275$ and $G_{L2} = 18.18$

$$D_{TG} = D_1 - D_I \tag{35}$$

Turn Anticipation.

Logic is used to anticipate the turn before the aircraft gets to the next waypoint. This action was found necessary to reduce the tracking error during transition to the circular leg. A distance, D_A, is computed based on a four second lead time. As the aircraft nears the next waypoint, the logic switches the roll steering command to a ramp to start the turn. This event occurs at point 1 in Figure 9. When the aircraft passes the line at point 2 in the figure, the roll steering command switches to the circular tracking signal. As this switching occurs, the variable D_1 is reset to the remaining distance to go. Also, the quantity D_I is set to zero at this time. These variables are now reinitialized properly for use in the next set of calculations.

Circular Leg Steering Commands.

Figure 10 shows the tracking error, ΔR , during the turn. The following equations define the roll steering command used for this leg. The reference course angle, ψ_R , defines the desired path direction during the turn. It is used to calculate the deviation from the ground track angle, Eqn (35), which in turn defines the error rate term $\Delta\dot{R}$.

$$C^2 = \left(x(i_S-1) - \hat{x}_m\right)^2 + \left(y(i_S-1) - \hat{y}_m\right)^2$$

$$\Delta R = I_R(i_S-1)\left\{R(i_S-1) - \left[\left(\hat{x}_m - x_c(i_S-1)\right)^2 + \left(\hat{y}_m - y_c(i_S-1)\right)^2\right]^{\frac{1}{2}}\right\} \tag{36}$$

$$\psi_R = \tan^{-1} \frac{\hat{x}_m - x_c(i_S-1)}{\hat{y}_m - y_c(i_S-1)}, \quad 0 \leq \psi_R < 2\pi \tag{37}$$

$$\Delta\dot{R} = V_G \sin(\psi_G - \psi_R) \tag{38}$$

$$\phi_{STR} = I_R(i_S-1) \tan^{-1} \frac{V_G^2}{32.2\ R(i_S-1)} - G_{L3}\Delta R - G_{L4}\Delta\dot{R} \tag{39}$$

where $G_{L3} = 0.01$ and $G_{L4} = 0.1$

The distance along the circular leg is computed next. This distance, D_I, is measured from the last waypoint to the point projected along the desired circular arc (Figure 10). The total distance to go is then computed from this leg distance.

$$A = \cos^{-1} \frac{\left[R(i_S-1) + \Delta R\right]^2 + R^2(i_S-1) - C^2}{2\left[R(i_S-1) + \Delta R\right] R(i_S-1)} \quad \text{rad}$$

$$D_I = R(i_S-1)A \tag{40}$$

$$D_{TG} = D_1 - D_I \tag{41}$$

Turn Termination.

As the aircraft approaches the next waypoint, logic is used to lead the transition to the linear leg similar to the turn anticipation. Point 1 in Figure 11 is calculated using a four second lead time. At this point, a signal is computed based on the next (linear) leg. This signal has the same form as the steering command, Eqn (33). The circular steering signal, Eqn (37), is still being used to command the bank angle during this time. At point 2, the linear signal and circular steering signals are equal in magnitude. At this time, the steering command is switched to the linear one, Eqn (33). Abrupt changes in the command signal are avoided by this logic. When point 3 is reached, the appropriate variables are reinitialized for the linear leg, and steering continues using Eqns (31)-(34).

VERTICAL GUIDANCE EQUATIONS

Generalization of the vertical guidance algorithm discussed in Reference 1 was made during this study. The concept employed allows the vertical tracking error to be computed by knowing only the parameters that define the current leg in which the aircraft is flying. A constant glideslope can be defined for each leg, or one glideslope change can be executed per leg.

One way to visualize this concept is to consider "straightening out" the approach path to lie in a single plane. The altitude is displayed vs the distance to go as depicted in Figure 12. A typical leg is shown as identified by waypoints $WP(\ell)$ and $WP(\ell-1)$. Altitudes at each waypoint are known, and the distance D_I is computed from Eqn (32) or Eqn (40) depending on whether a linear or circular leg is the current leg. Each waypoint has associated with it two glideslopes. (They may have equal or different values.) Consider the situation in Figure 12 where the aircraft is below the first glideslope for leg ℓ. The desired altitude, h_d, for this glideslope is computed from

$$h_D = h(\ell) - D_I \tan G_S(\ell,1) \tag{42}$$

After the aircraft has progressed to the region of the second glideslope as shown in Figure 13, the desired altitude is given by

$$h_D = h(\ell-1) + \left[D_L(\ell) - D_I \right] \tan G_S(\ell,2) \tag{43}$$

Deviation from the desired altitude is defined by

$$\Delta h = h_D - \hat{h}_m \tag{44}$$

The error rate signal is derived from rate and acceleration signals. Figure 14 is the block diagram that contains a complementary filter that provides this error signal. Filtered altitude rate, $\dot{h}_F$, is a signal available in the MD-80 autopilot. It is used to develop filtered altitude rate error, $\hat{\dot{h}}$, as defined by the following difference equations that are equivalent to the continous system of Figure 14:

$$\hat{\ddot{h}} = -\left[\dot{h}_F - \dot{h}_{F-} \right] / \Delta T$$

$$\Delta z_1 = C_1 \, \Delta z_{1-} + C_3 \hat{\ddot{h}} \tag{45}$$

$$\Delta z_2 = C_1 \, \Delta z_{2-} + C_2 \left[\Delta h - \Delta h_- \right]$$

$$\Delta \hat{\dot{h}} = \Delta z_1 + \Delta z_2 \tag{46}$$

$$C_1 = e^{-\Delta T/\tau} \qquad (\tau = 4.0 \text{ sec})$$

$$C_2 = \tau \; 1 - e^{-\Delta T/\tau}$$

$$C_3 = \; 1 - e^{-\Delta T/\tau} \; / \Delta T$$

As shown in Figure 14, the pitch command signal to the autopilot, θ_{CE} , is composed of three components. The pitch steering signal is a combination of the altitude error and rate signals:

$$\theta_{STR} = G_{V2} \Delta h + G_{V4} \hat{\dot{h}} \tag{47}$$

where $G_{V2} = 0.0588$ and $G_{V4} = 0.294$

An integral term, θ_{CI} , is used on the Δh signal, and a predict term, θ_P , is used when switching from one glideslope to another. This predict term is computed from the vertical flight path angle, γ , at the time of switching.

$$\theta_{CI} = \theta_{CI-} + G_{V3} \Delta h \Delta T \tag{48}$$

where $G_{V3} = 0.00294$

$$\gamma = \tan^{-1} \frac{\dot{h}_F}{V_G} \tag{49}$$

$$\theta_P = \theta_{P-} + \gamma - G_S(\ell, 2) \tag{50}$$

$$\theta_{CE} = \theta_{STR} + \theta_{CI} + \theta_P \tag{51}$$

Switching to the second glideslope is determined by logic based on the second glideslope parameters. This signal is computed while the aircraft is still tracking the first glideslope. When this signal changes sign, switching occurs with a smooth transition to the second glideslope. The flow diagram for the vertical guidance subroutine is shown in Figure 15.

SPEED CONTROL

Programmed speed and flap changes were simulated during leg 10 of the river approach. This choice was somewhat arbitrary, but it was made so that the speed change would be on the linear leg after the second turn. The result is the speed transient settles out before the next turn.

Speed control is simply implemented by commanding a step flap change to the flap servo, and a step speed change to the autothrottle. All existing logic and limits in the MD-80 autothrottle remain unaltered. The result is a flap change from 15 deg to the desired setting of 40 deg at the max servo rate. A speed change from 165 knots to the target speed of 140 knots accompanies this flap change.

SIMULATION DESCRIPTION

MD-80 SIMULATION PROGRAM

A modified version of the MD-80 batch simulation program was used for the river approach studies, where the ILS subroutines were replaced with coding that simulated the MLS angle and range signals. Routines for lateral and vertical guidance and speed change were developed and added to the program to provide a closed loop simulation capability. Figure 16 shows the relationship of the basic elements of the simulation. The roll and pitch inner loops of the MD-80 autopilot accept commands from the MLS guidance computer. Surface commands generated within the autopilot provide the desired lateral and vertical path tracking control for the approach.

Another mode of operation is possible where the autopilot is replaced with a flight director. A pilot would then fly the MLS approach and would make the necessary lateral, vertical, and speed maneuvers. A simulator is planned to be used in future pilot-in-the-loop evaluations of MLS approach procedures, pilot displays, and path tracking performance. The last sections of this report discuss some aspects of hardware interfaces and software requirements of the fixed-base simulator.

WIND AND TURBULENCE MODELS

Included in the simulation are options for winds, whose magnitudes are a function of altitude, and for turbulence as additive terms to the winds. The factor that is a function of altitude is denoted W and is defined by

$$W = 0.43 \log h + 0.35 \tag{52}$$

where h is the altitude in feet. Input values for S_x, S_y, and S_z (the wind magnitudes in knots) when the airplane is on the ground are used to compute the three wind components at altitude:

$$\begin{aligned} W_x &= W\ S_x \\ W_y &= W\ S_y \\ W_z &= W\ S_z \end{aligned} \tag{53}$$

Turbulence is a random variable that may be added to the above winds. White noise is passed through first order filters whose parameters are functions of the wind components as shown in Figure 17. Outputs of the filters are denoted U_g, V_g, and W_g and are used to form the total simulated winds:

$$W_{Tx} = W_x + U_g$$
$$W_{Ty} = W_y + V_g$$
$$W_{Tz} = W_z + W_g$$

Aircraft performance characteristics limit wind components at touchdown to maximum values of 25 knot headwinds, 10 knot tailwinds, and 15 knot crosswinds.

WINDSHEAR

One case was simulated in which a severe windshear was present during the final approach at Washington. This shear was based on the Logan/Iberia incident of 1973. The data (published by Aviation Week in 1975 (Reference 2)) was modified for simulation purposes and appears in Table 3. Linear interpolation was used to define the shear between the altitudes listed.

MLS NOISE MODELS

Angle and range signals as output from the MLS receiver will contain noise. For simulation purposes, additive noise has been included in the azimuth, elevation, and DME range variables θ_{AZ}, θ_{EL}, & R_{DME} respectively. The variables, as used in Equation (1) - (3), were modified to include this additive noise:

$$\theta_{AZ} = \theta_{AZ(TRUE)} + \theta_{AZ(NOISE)}$$
$$\theta_{EL} = \theta_{EL(TRUE)} + \theta_{EL(NOISE)}$$
$$R_{DME} = R_{DME(TRUE)} + R_{DME(NOISE)}$$

The International Civil Aviation Organization (ICAO) has specified noise levels for which the MLS must meet. These levels, as defined by 2σ or 95% probability values, are given in Table 4. Values for the low frequency path following error (PFE) and the high frequency control motion noise (CMN) are specified for AZ, EL, and DME/P.

The ICAO-specified noise levels, if actually present in the MLS signals, would result in unacceptable aircraft activity when coupled to flight control systems capable of accurate path control. Flight measurements indicate that the noise is less. Consequently, assumed levels of reduced value were simulated. These reduced levels were based on actual flight test data performed in France in 1983 (Reference 3). Results of these tests were used to define the gains and frequencies shown in Figure 18. For simulation purposes, 1σ or 68% probability values are used. The reduced values shown in Table 4 were used to obtain the noise model of Figure 18. Azimuth and elevation levels are significantly lower than the ICAO values, whereas the DME level remains unchanged.

During the course of the present study, two baseline cases were run with no noise for comparison purposes. All other cases contained the reduced noise. For certification purposes, the ICAO values must be used. However, it was felt that noise models, based on actual flight test data, would yield results representing levels encountered in actual practice.

SIMULATION RESULTS

Two sets of runs were executed for the river approach. In the first set, four runs simulated entry to the approach at approximately 3000 feet altitude. In the second set, six runs simulated the final approach starting at 1700 feet and ending at 100 feet. Pitchover and a speed change were programmed at the higher altitude to study their effects on tracking. Tracking accuracy was of particular interest for the second set of runs in the presence of turbulence and shear.

ENTRY APPROACH RESULTS

Results for the initial path approach are presented for four cases as defined in Table 5. Specifically, the path starts at WP(14) (Figure 4) and ends on leg 10 after WP(10). Leg 14 is at a constant altitude. Pitchover to a 3 degree glideslope occurs at ENTRY. Thereafter, a constant 3 degree descent is maintained.

Case 1.

This is a baseline case with no noise or other disturbance. Bank angle time history as shown in Figure 19 has the waypoints identified along the time axis. Note that the bank angle starts to change before WP(13) and WP(11). Turn anticipation accounts for this effect since the waypoints are defined at the time of switching from the linear steering command to the circular steering command.

Pitchover occurs at 20 sec, with the pitch response shown in Figure 20. There are pitch corrections at each waypoint to account for the turning aircraft. As expected, a smooth transition between waypoints occurs, accompanied by a smooth pitchover to the desired glideslope. This part of the approach poses no particular problems to the guidance algorithms.

The lateral tracking error is shown in Figure 21. Discontinuities in this trace are due to switching of the steering signal at each waypoint. This plot is a composite of the Δy error, Eqn (31), and the ΔR error, Eqn (36). These errors, and their respective rates, are used to define the lateral steering command. Since this case has no disturbances, these errors are inherent in

the MD-80 and are due to the aircraft dynamics, autopilot inner loops, and limits in the autopilot.

Figure 22 shows a time history of the vertical tracking error. At pitchover, the aircraft is about 65 feet below the desired altitude. This transient settles out to within a few feet for the remainder of the run, with some correction during the turns. Figure 23 is a plot of vertical descent rate. After transients, this rate is close to the -12.4 feet/sec nominal value for this descent.

A computer-generated plot of the ground track for Case 1 is shown in Figure 24. The dashed line connects the named waypoints and the solid line is the ground track. At the scale shown, the tracking errors are not obvious. This type of plot will be useful for cases with wind and turbulence when the track is plotted using an expanded scale.

Case 2.

Results for the MLS noise case differ from the baseline primarily in the vertical plane. Lateral tracking is minimally affected. (See Figures 25 and 26.) Pitch response (Figure 27) shows the effect of the vertical tracking error (Figure 28) which contains the noise components. It should be noted that drawing conclusions using a single noise run is not valid. The trend, however, in pitch response after the turns does show approximately a ± 0.5 degree dispersion about the nominal. Vertical tracking error shows a ± 20 foot dispersion during the same period. Vertical descent rate, Figure 29, has a ± 2 ft/sec spread about nominal after the pitchover to 3 degrees.

Case 3.

A headwind and a crosswind were simulated as a function of altitude for this case. The magnitudes at threshold were 25 knots for the headwind and 15 knots for the crosswind. At the initial altitude of 3146 feet, these values (as modified by Eqn (52)) become 46 and 28 knots, respectively.

The bank angle time history of Figure 30 shows a smaller angle achieved during the first turn (between WP(13) and WP(12)). This reduction is a result of the decreased ground speed due to the wind. About a 30% reduction in this speed had occurred at the end of the first turn as compared to the no-wind case.

Without wind, a 50 foot error to the left of the desired track developed at the end of the first turn (Figure 26).

Since the bank angle was smaller with these particular winds, the tracking error was actually less (15 feet) because the aircraft did not turn as sharply (Figure 31). Had the wind direction been reversed, the opposite situation would have occurred. Tracking errors are very dependent on the relative wind direction, and in some cases the errors are reduced while in other cases they are increased. At the end of the second turn (WP(10)), the wind case shows a smaller error than the no-wind case. A 40 degree course change had occurred between the first and second turns. Consequently, the wind direction was favorable to cause the aircraft to track more closely.

This particular wind condition was actually selected for the final approach cases. There is a restricted area near WP(5) and a crosswind from the right is a worst-case condition.

Case 4.

This last case for the initial approaches is a programmed speed change and a configuration change. Initially, the speed is 165 knots and the flap setting is 15 degrees. On leg 10, the speed is reduced to 140 knots and the flaps are extended to 40 degrees. The major effect on bank angle is to increase the commanded angle because of the higher speed (Figure 32). Both turns occur at 165 knots. The lateral tracking error (Figure 33) is generally smaller as compared to the constant speed case, whereas the vertical tracking error is about the same. The speed and flap change commands occur slightly before 80 seconds, and the speed change is smooth (Figure 34).

TERMINAL AREA APPROACH RESULTS

Results for the remaining six cases as defined in Table 5 are presented. For these cases, the initial position of the aircraft is on leg 10 and descending along a 3 degree glideslope. Four turns are executed during this final approach. Two additional effects studied for these cases are the addition of turbulence to the steady winds and a windshear profile.

These six cases were simulated down to a 100-foot decision height. At this point, the tracking errors were recorded and the speed error noted. Results are shown in Table 6. It must be pointed out that results for the cases containing noise or turbulence are random in nature. To obtain an accurate picture, one should process many runs to obtain a statistical dispersion. Time did not permit this processing during the present study. An alternate way of assessing performance of random disturbances is to compare time histories of the various cases. Relative dispersions over a reasonable time period can give some insight into the tracking performance.

Case 5.

This case is similar to Case 1 in that no noise or disturbances are present. Bank angle time history is shown in Figure 35, where the waypoints are identified on the time axis. Note that waypoints 5 and 4 are spaced only a few seconds apart. Consequently, the turns during this time are almost an S-turn type of maneuver.

Pitch response, Figure 36, shows a ± 1 degree variation in angle due to the coupling from roll. For the initial approach cases, the variation was about ± 0.5 degree. More closely-spaced turns cause more pitch activity.

Lateral tracking error, shown in Figure 37, is on the same order of magnitude as Case 1. Vertical errors of Figure 38 reflect the larger pitch variation and are about twice those in Case 1. Due to the expanded scale of the descent rate (Figure 39), the excursions appear to be large. Actually, they are on the same order of magnitude as the descent of Case 1 after the pitchover has occurred. The ground track for this case from the initial point to threshold is shown in Figure 40.

Case 6.

As in Case 1, the effect of MLS noise is seen in increased vertical errors with about the same lateral errors (Figures 41-45). Dispersion in pitch tracking error is about double that of the no-noise case (± 15 ft vs ± 7 ft). This same level of MLS noise is used in the remaining cases.

Cases 7 and 8.

The same headwind and crosswind (scaled by altitude) as used in Case 3 was used in Case 7. In addition, turbulence, as defined in Figure 17, was added to the wind for Case 8.

Lateral tracking errors are compared for these two cases in Figure 46. Although the shapes of these two curves are different than the no-wind case (Case 5), the excursions are about the same. For the vertical plane, Cases 7 and 8 are compared in Figure 47. Here, the comparison to the no-wind case shows an increase in excursion of a factor of 3 to 4. The steady wind values used in the simulation were somewhat severe. Since the RMS levels of the turbulence are functions of these steady wind levels, turbulence is also severe. Nevertheless, the expanded scale ground track shown in Figure 48 shows a reasonable trace. Case 8 results produced no problems in flying near a restricted area, which is located about 1500 feet from leg 4 (the last leg before FAF18).

Case 9.

Windshear components used for this case are shown in Table 3. Positive values represent tailwinds and crosswinds from the right. The main effect of this windshear is to appreciably increase the bank angle required for the turns (up to 25 degrees as shown in Figure 49). The lateral tracking error, Figure 50, is about the same as Case 6. Vertical tracking error (Figure 51) increased to about 25 feet during the first part of the approach, with an increase up to 30 feet near the change to a headwind (between 300 and 400 feet altitude). This increase represents a factor of 2 as compared to the error in Case 6.

Case 10.

This case represents a minimum-weight landing configuration. It is the same as Case 6 except for the weight and speed differences (See Table 5). As noted in Table 6, the error at the 100 foot altitude point are the same as the full-weight case. Peak error (Figure 52) was slightly higher (200 feet) at 80 seconds as compared to a 50 feet peak for Case 6.

FIXED BASE SIMULATOR CONSIDERATIONS

A logical extension to the current MLS guidance system simulation studies is a man-in-the-loop, real-time simulation evaluation. This task would involve taking the algorithms developed during the present study and revising them as necessary for use in a real-time environment. A fixed-base simulator that includes MD-80 autopilot and Performance Management System (PMS) hardware is available for this purpose. Interfaces between this hardware and the computer simulation program need to be established.

The first step in identifying these interfaces is to note what inputs and outputs are associated with the algorithms. Table 7 is a signal computation diagram containing a review of the major input/output and computations performed by the lateral computer program. Table 8 is a similar diagram for the vertical guidance program. These tables indicate the basic signal generation and inputs necessary for their computation.

Figure 53 is a simplified block diagram showing the interconnections between the MLS guidance computer and the other aircraft systems. The new MLS guidance functions will have to interface properly with the hardware that is included in the simulator and with the existing software. Tasks were identified in the Recommendations section that relate to this interfacing follow-on effort.

REFERENCES

1. J. B. Feather: Guidance Studies for Curved, Descending Approaches Using the Microwave Landing System (MLS), NASA CR-178030, May 1986.

2. Aviation Week and Space Technology, NTSB Assays Iberia Accident at Logan, April 7, 1975, Pg. 58.

3. Aviation Week and Space Technology, Thomson - CSF to Offer MLS Landing Aid, April 8, 1985, Pg. 79.

TABLE 1 - WASHINGTON NATIONAL RIVER WAYPOINTS

WAYPOINT NAME	x Ft.	y Ft.	Alt Ft.	Turn Radius Ft.
ENTRY	-44603.	36527.	3146.	9000.
CABIN	-40951.	26491.	3146.	8000.
WINDY	-18426.	15014.	1353.	7500.
KEYBR	-16425.	6990.	948.	6500.
MEMBR	-10827.	4014.	628.	7000.
FAF18	-5500.	0.	285.	7000.
GPI18	0.	0.	0.	---

TABLE 2 - TRANSFORMED RIVER WAYPOINTS

WAYPOINT NUMBER	$x(i_s)$ Ft.	$y(i_s)$ Ft.	$h(i_s)$ Ft.
1	-1908.1	0.	100.
2	-3157.9	0.	165.5
3	-7370.5	1409.5	402.39
4	-10387.	3682.4	600.33
5	-11314.	4272.7	657.98
6	-13870.	5631.5	809.68
7	-17125.	9798.1	1095.0
8	-17599.	11698.	1197.7
9	-21471.	16566.	1533.8
10	-38143.	25060.	2514.4
11	-42029.	29453.	2829.1
12	-43632.	33860.	3074.8
13	-46928.	38155.	3146.0
14	-48535.	39280.	3146.0

TABLE 3 - VALUES FOR SIMULATED WINDSHEAR

ATTITUDE FT.	TAILWIND/HEADWIND KNOTS	CROSSWIND KNOTS
5000.00	23.00	-26.00
1000.00	23.00	-26.00
800.00	22.00	-25.00
600.00	20.00	-24.00
500.00	18.00	-23.00
400.00	12.00	-17.00
300.00	6.00	-12.00
200.00	-3.00	-4.00
100.00	-6.00	-2.00
0.00	-4.00	-2.00

TABLE 4 - MLS NOISE MODELS (2σ or 95% PROBABILITY)

	AZIMUTH	ELEVATION	DME
ICAO VALUES	PFE = 0.104 DEG ($\pm$20 FT) CMN = 0.0548 DEG ($\pm$10.5 FT)	PRE = 0.133 DEG ($\pm$2 FT) CMN = 0.0663 DEG ($\pm$1.0 FT)	PFE = 100 FT CMN = 60 FT
REDUCED VALUES	PFE = 0.0312 DEG ($\pm$6 FT) CMN = 0.0208 DEG ($\pm$4 FT)	PFE = 0.018 DEG ($\pm$0.30 FT) CMN = 0.012 DEG ($\pm$0.20 FT)	PFE = 100 FT CMN = 60 FT

PFE = PATH FOLLOWING ERROR

CMN = CONTROL MOTION NOISE

RUNWAY LENGTH = 10,000 FT

TABLE 5 - SIMULATED CASE CONFIGURATIONS

CASE	SPEED (KNOTS)	WEIGHT (LB)	MLS NOISE	STEADY WIND	TURB	WIND SHEAR	PATH
1	140	132,000	NO	NO	NO	NO	
2	"	"	YES	"	"	"	
3	"	"	"	YES	"	"	INITIAL
4	165/140	"	"	NO	"	"	
5	140	"	NO	"	"	"	
6	140	"	YES	"	"	"	
7	"	"	"	YES	"	"	
8	"	"	"	"	YES	"	FINAL
9	"	"	"	NO	NO	YES	
10	116	90,000	"	"	"	NO	

TABLE 6 - TRACKING ERRORS AT 100 FT DECISION HEIGHT

CASE	VERTICAL ERROR FT	LATERAL ERROR FT	SPEED ERROR KT
5	2	50	< 0.5
6	2	50	< 0.5
7	12	30	3
8	12	10	9
9	20	30	3
10	2	50	< 0.5

TABLE 7 - LATERAL GUIDANCE SIGNAL COMPUTATION DIAGRAM

INPUTS		OUTPUTS
MLS Angles, Range: $\theta_{AZ}, \theta_{EL}, R_{DME}$	$\Rightarrow$	MLS Position Coordinates: x_m', y_m', h_m'
Waypoint Data: x, y Turn Radius: R	$\Rightarrow$	Desired Course Angle: ψ_D Leg Distance: D_{LG} Total Distance To Go: T_{DLG}
Inertial Acceleration From Existing Filters: $\ddot{x}, \ddot{y}$	$\Rightarrow$	Filtered MLS Position and Date Signals: $(\hat{x}_m', \hat{y}_m'), (\hat{\dot{x}}_m, \hat{\dot{y}}_m)$
		$\Downarrow$
		Ground Track Angle: ψ_G Transformed MLS Position: $\hat{x}_m, \hat{y}_m, \hat{h}_m$ Ground Speed: V_G Course Deviation and Rate: $\Delta y, \Delta\dot{y}$ Roll Steering Command: ϕ_{STR} Distance to Go: D_{TG}

TABLE 8 - VERTICAL GUIDANCE SIGNAL COMPUTATION DIAGRAM

INPUTS		OUTPUTS
Waypoint Data: h, G_S Leg Distance: D_{LG}	$\Rightarrow$	Desired Altitude: h_D Altitude Error: Δh
Altitude Rate and Acceleration From Existing Filters: $\dot{h}_F, \hat{\ddot{h}}$	$\Rightarrow$	Altitude Error Rate: $\Delta\hat{\dot{h}}$
		$\Downarrow$
		Pitch Steering Signal: θ_{STR} Vertical Flight Path Angle: γ Pitch Steering Command: θ_{CE}

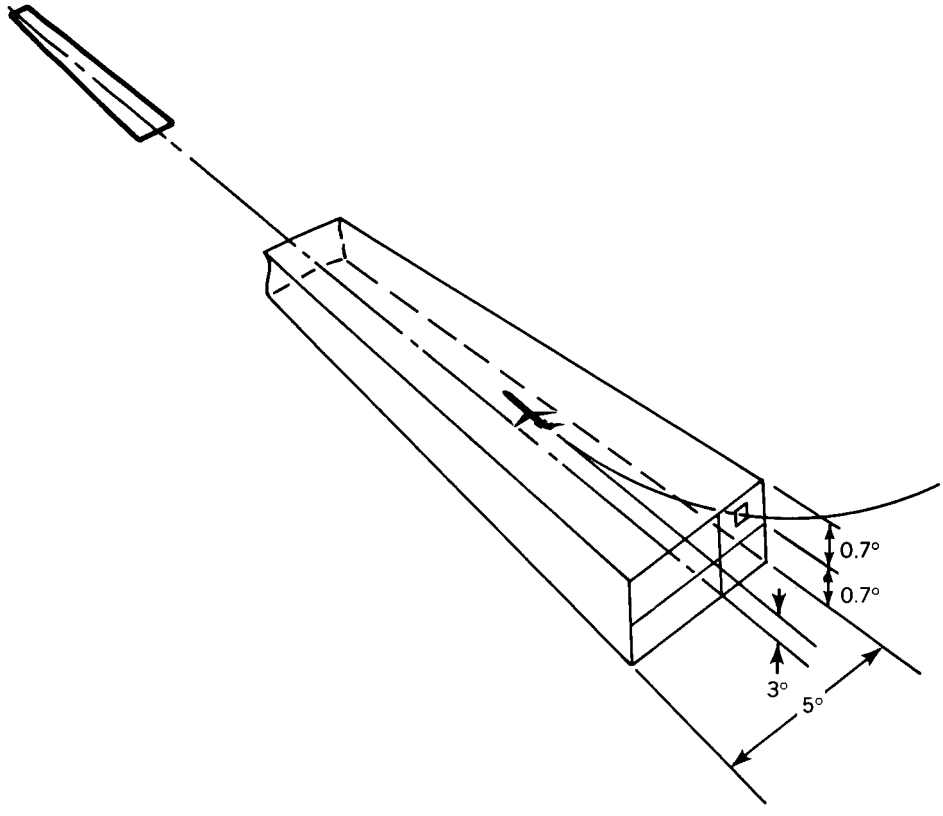

Figure 1. Existing ILS Coverage

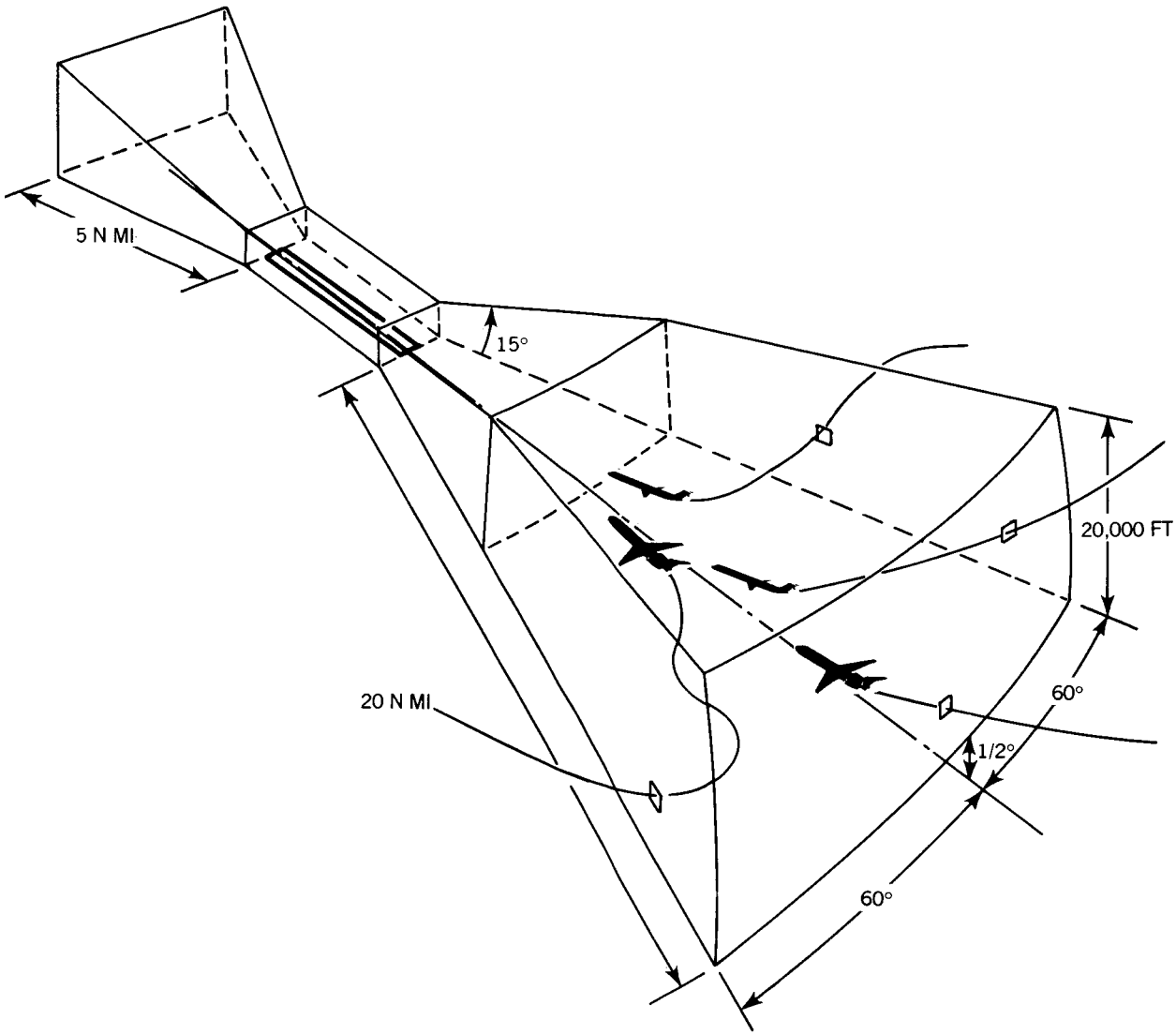

Figure 2. Extended Coverage Possible with MLS

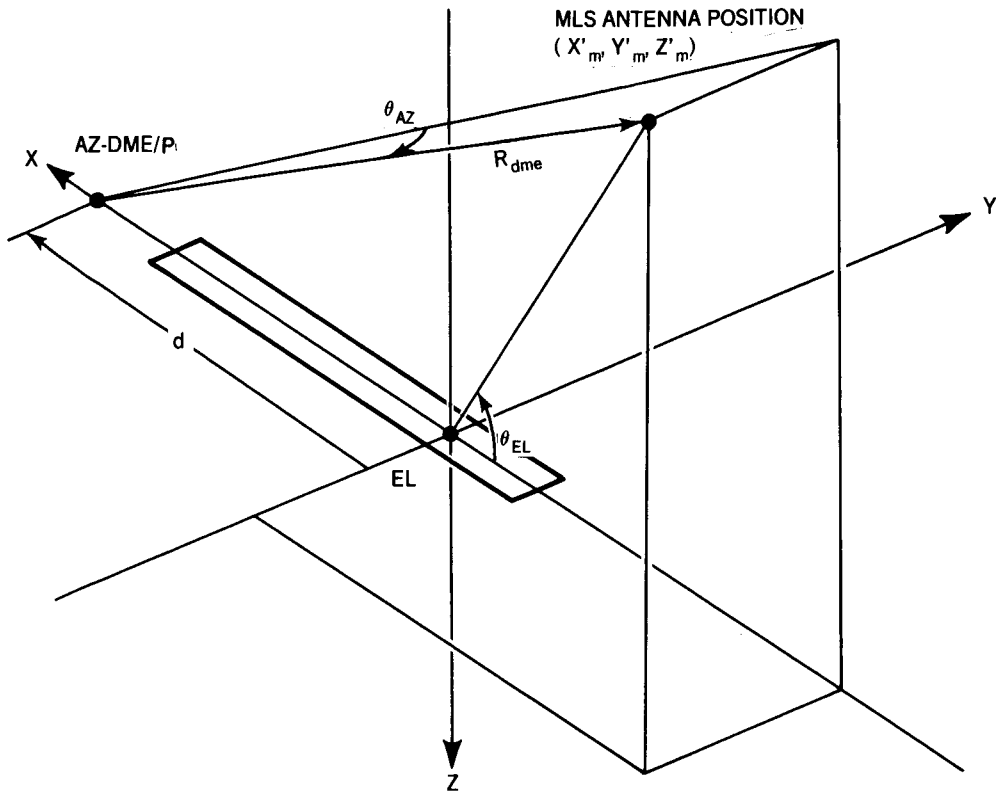

Figure 3. MLS Approach Geometry

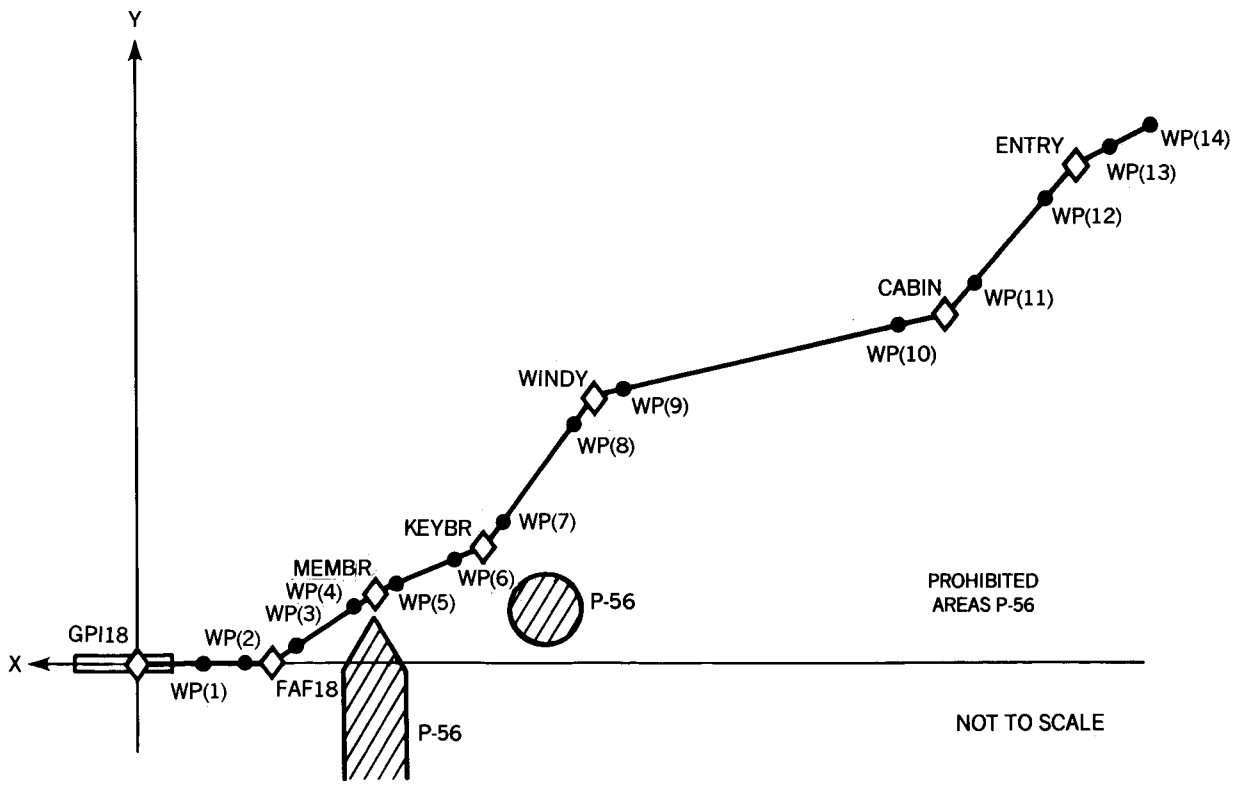

Figure 4. Waypoints for Washington National River Approach

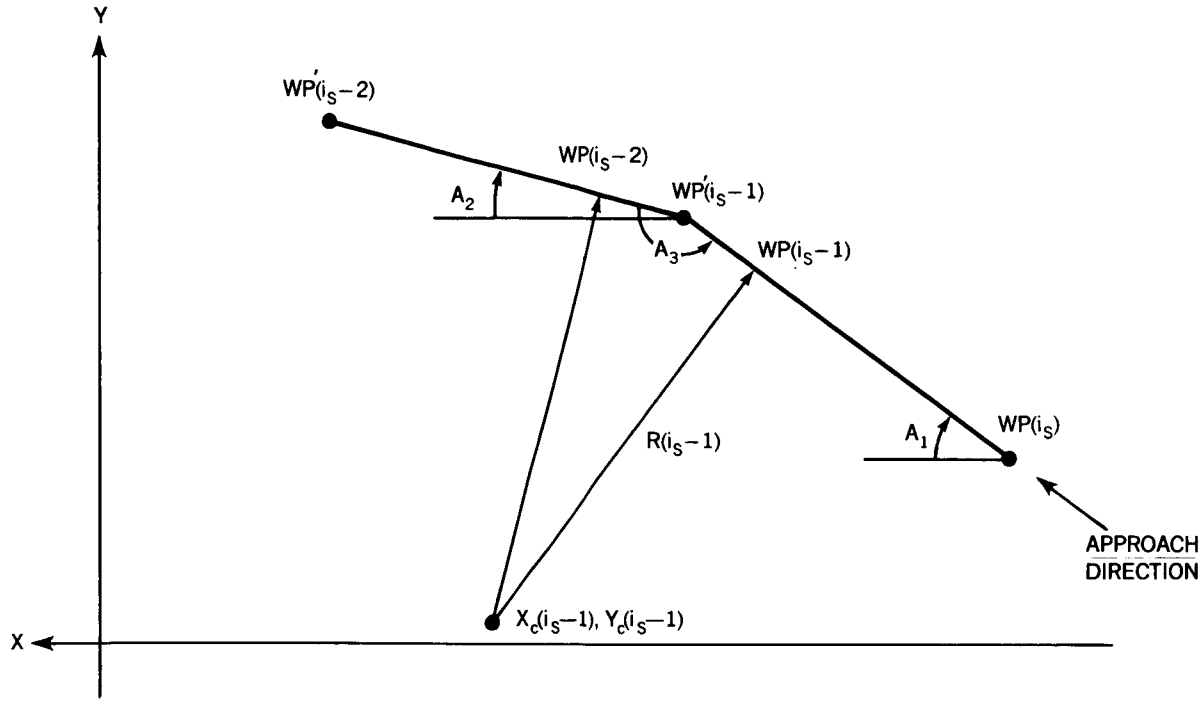

Figure 5. Waypoint Transformation Geometry

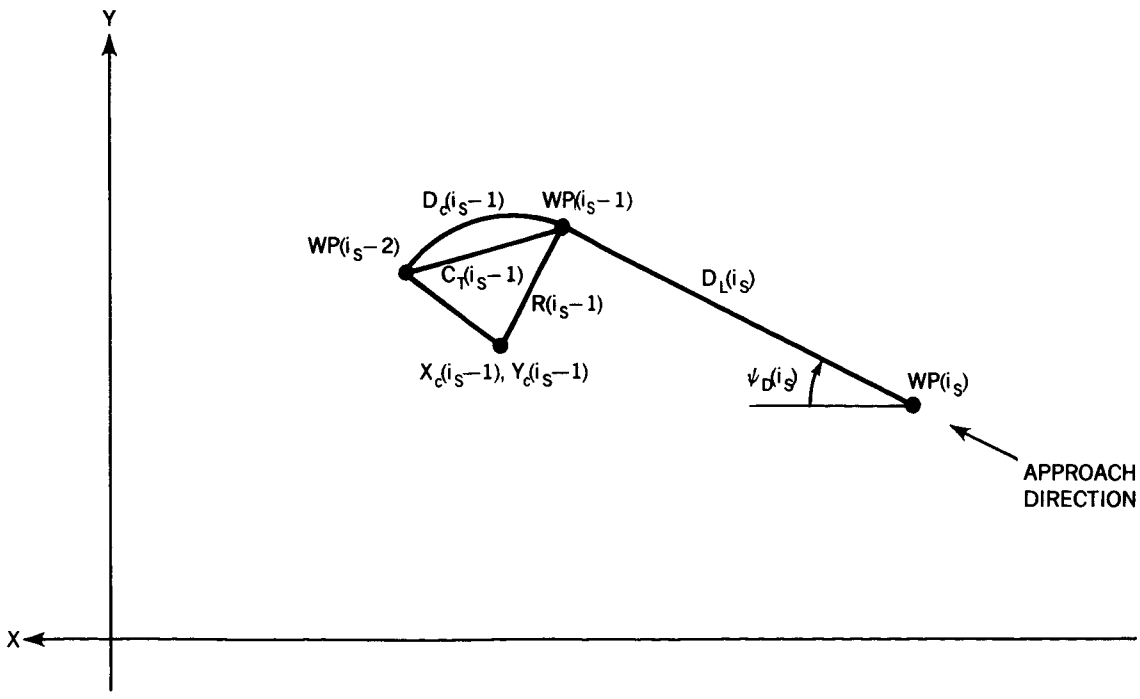

Figure 6. Lateral Guidance Geometry

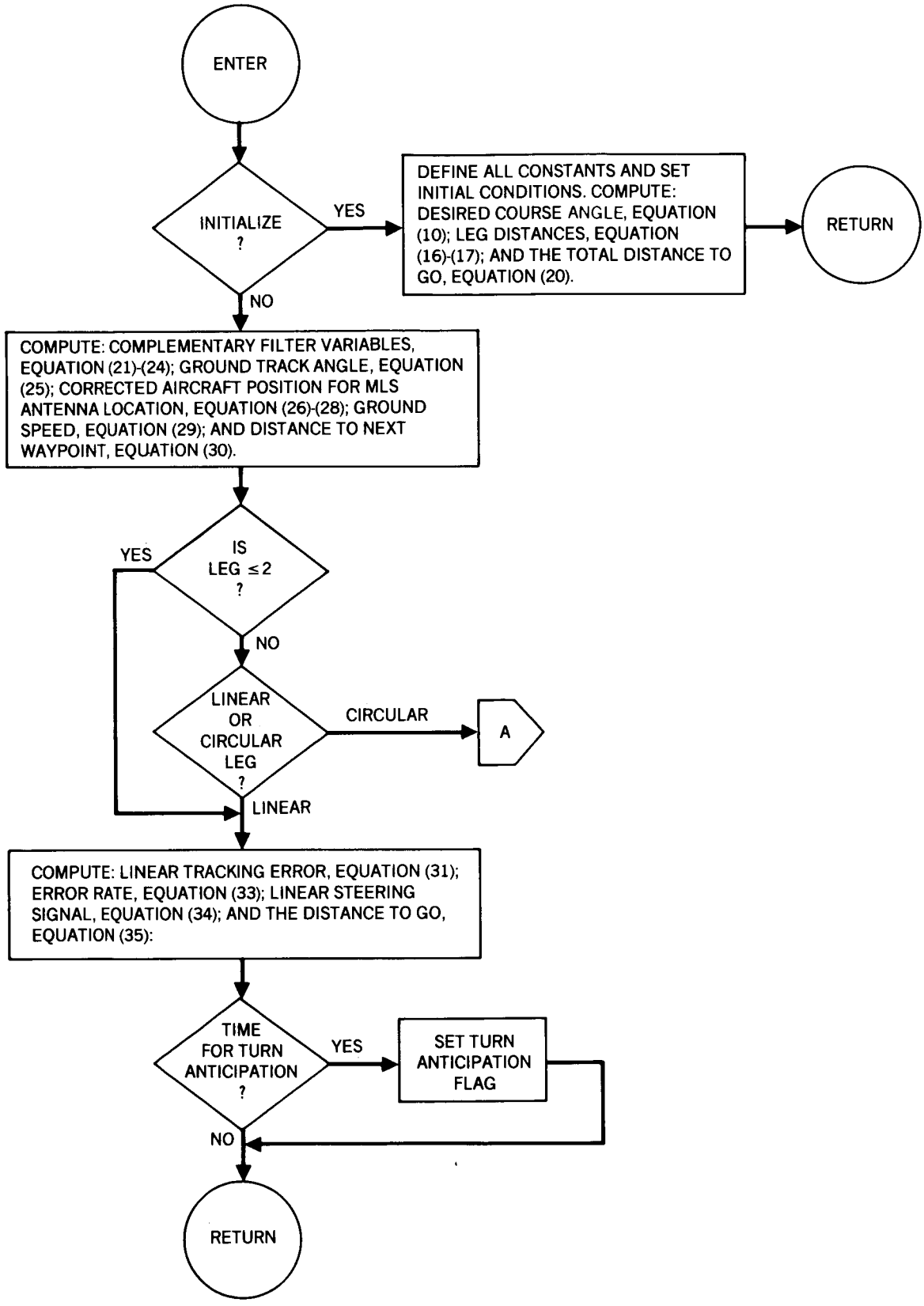

Figure 7. Lateral Guidance Flow Digram (Sheet 1)

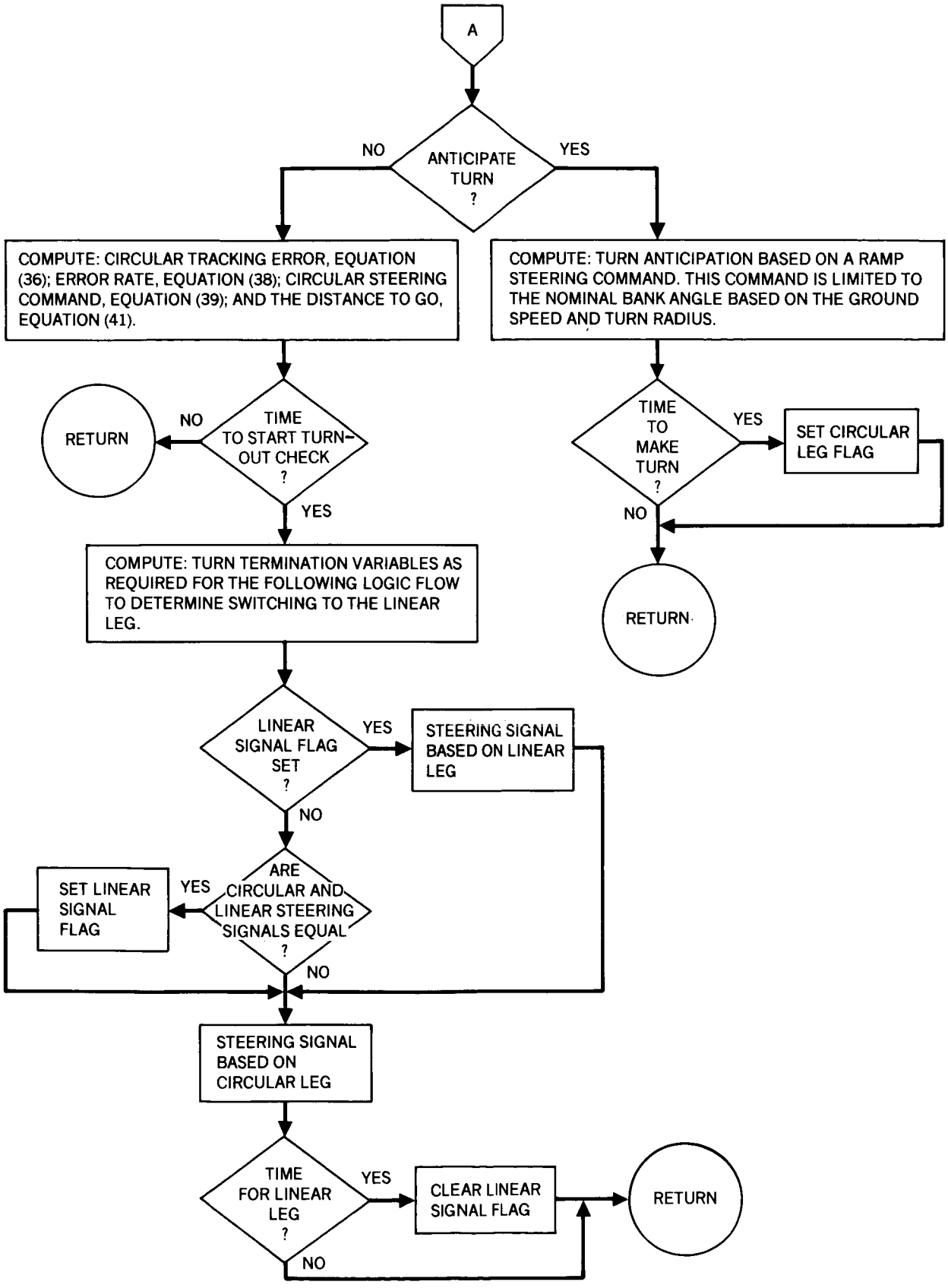

Figure 7. Laternal Guidance Flow Diagram (Sheet 2)

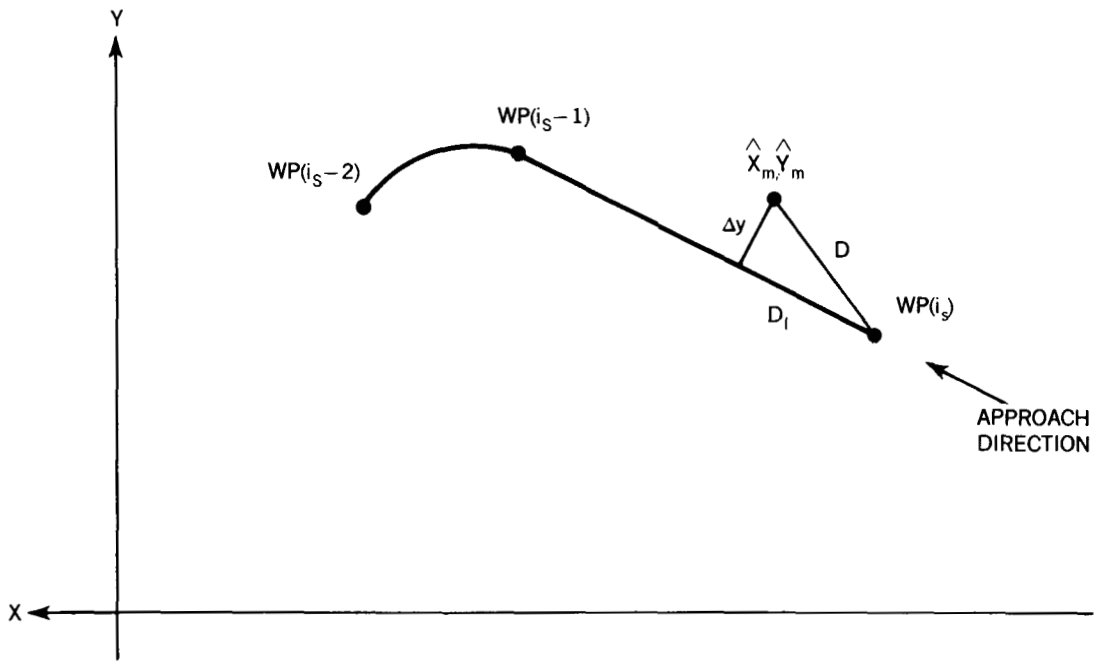

Figure 8. Lateral Tracking Error for Linear Leg

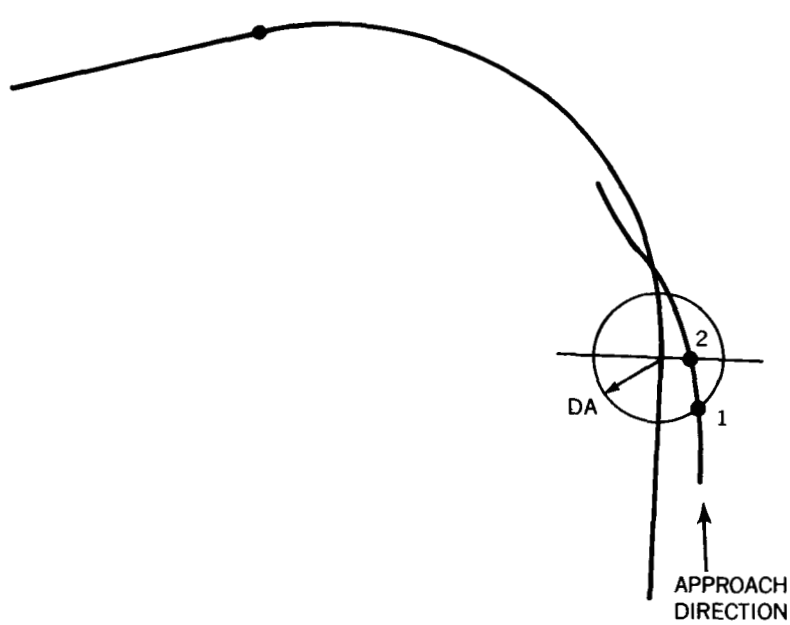

Figure 9. Turn Anticipation Geometry

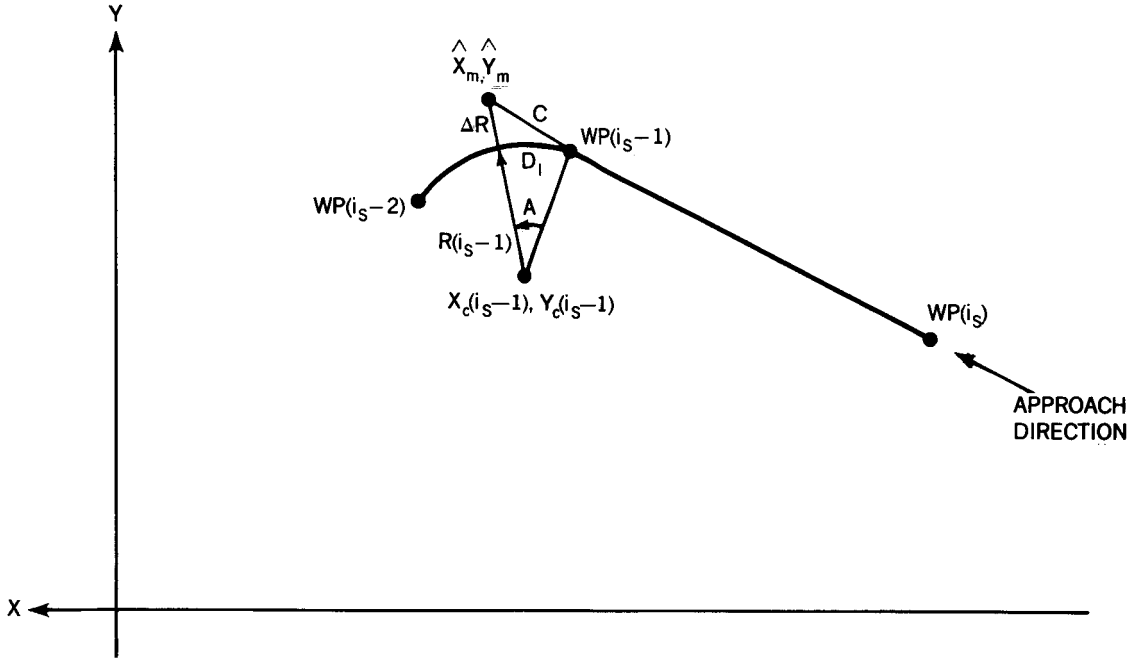

Figure 10. Lateral Tracking Error for Circular Leg

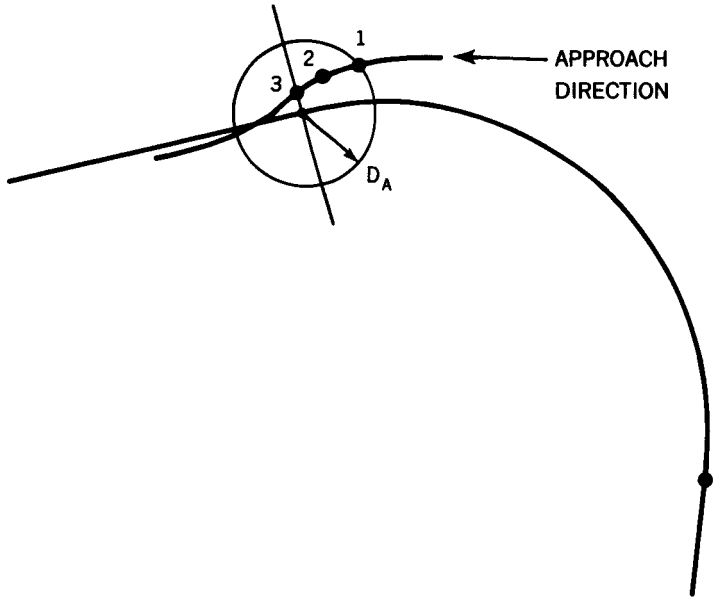

Figure 11. Turn Termination Geometry

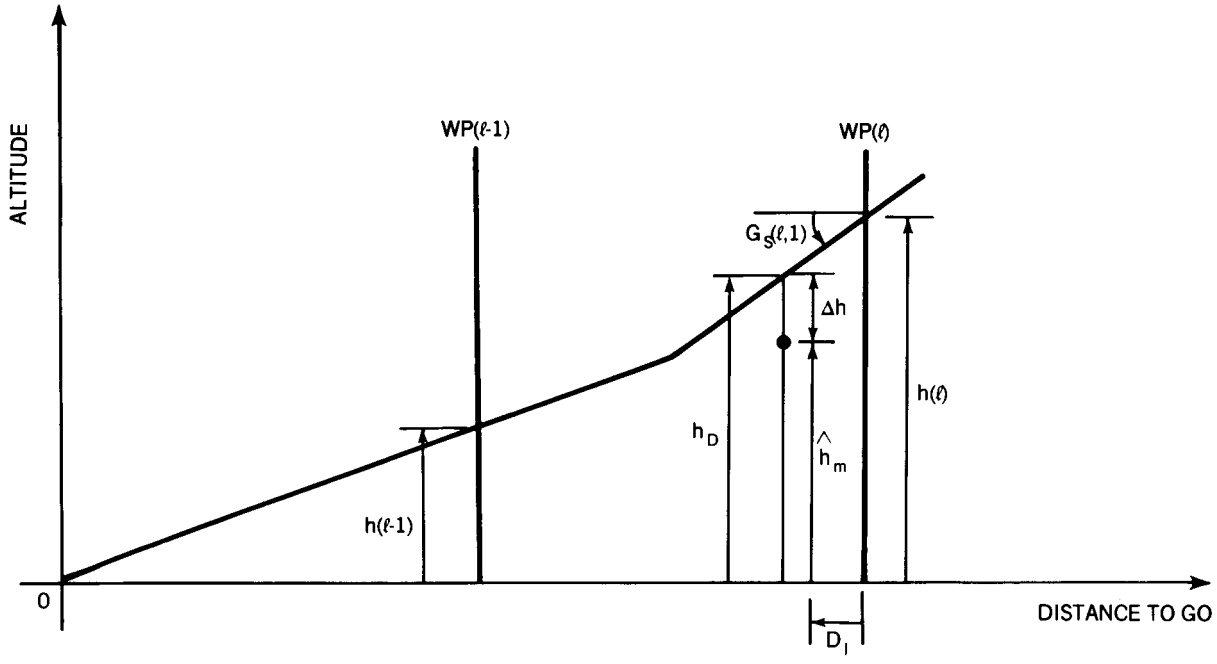

Figure 12. Vertical Tracking Error for First Glideslope

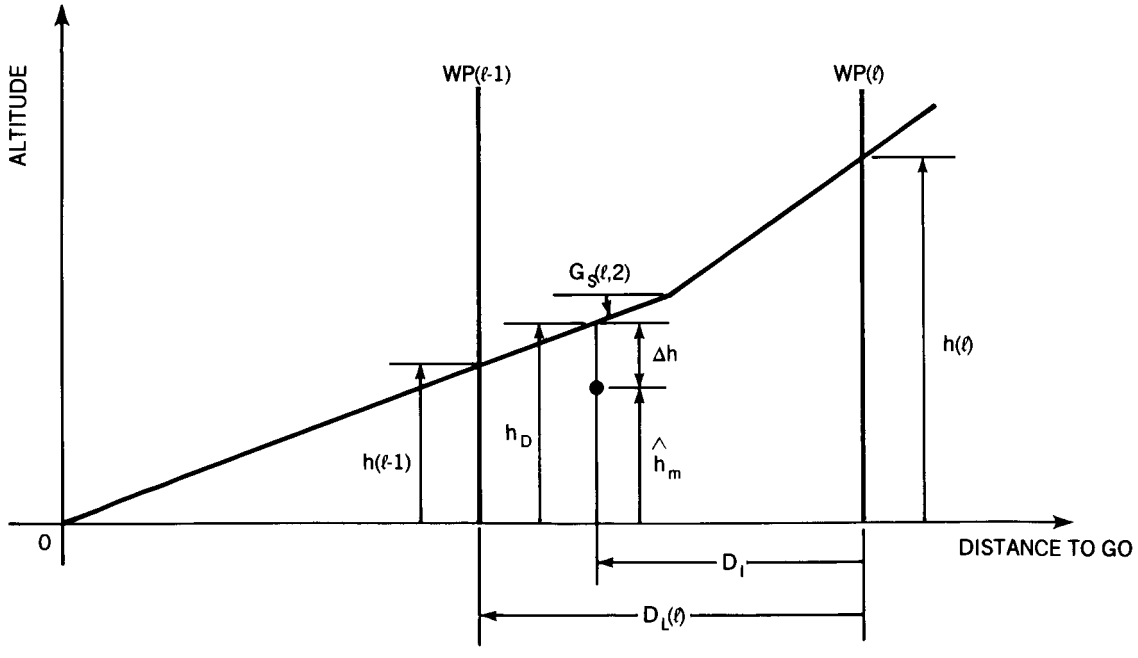

Figure 13. Vertical Tracking Error for Second Glideslope

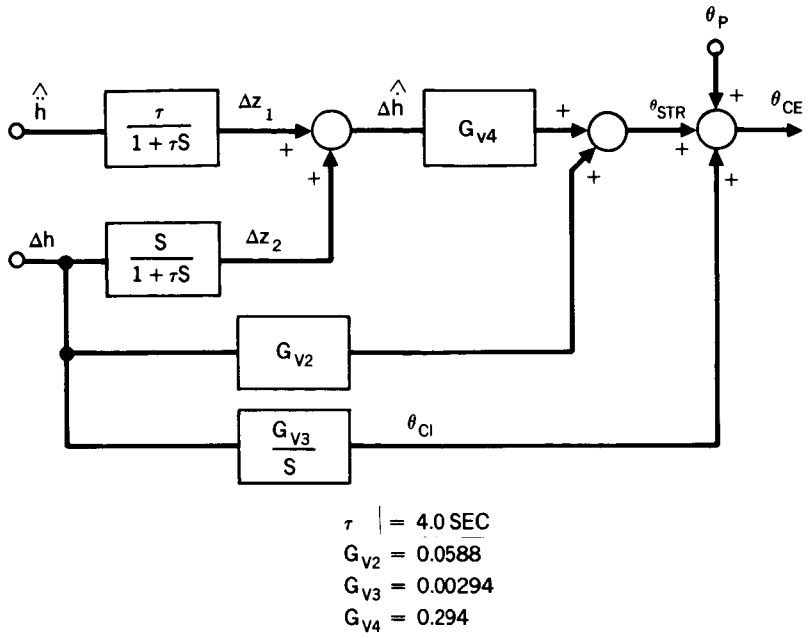

Figure 14. Block Diagram of the Vertical Steering Algorithm

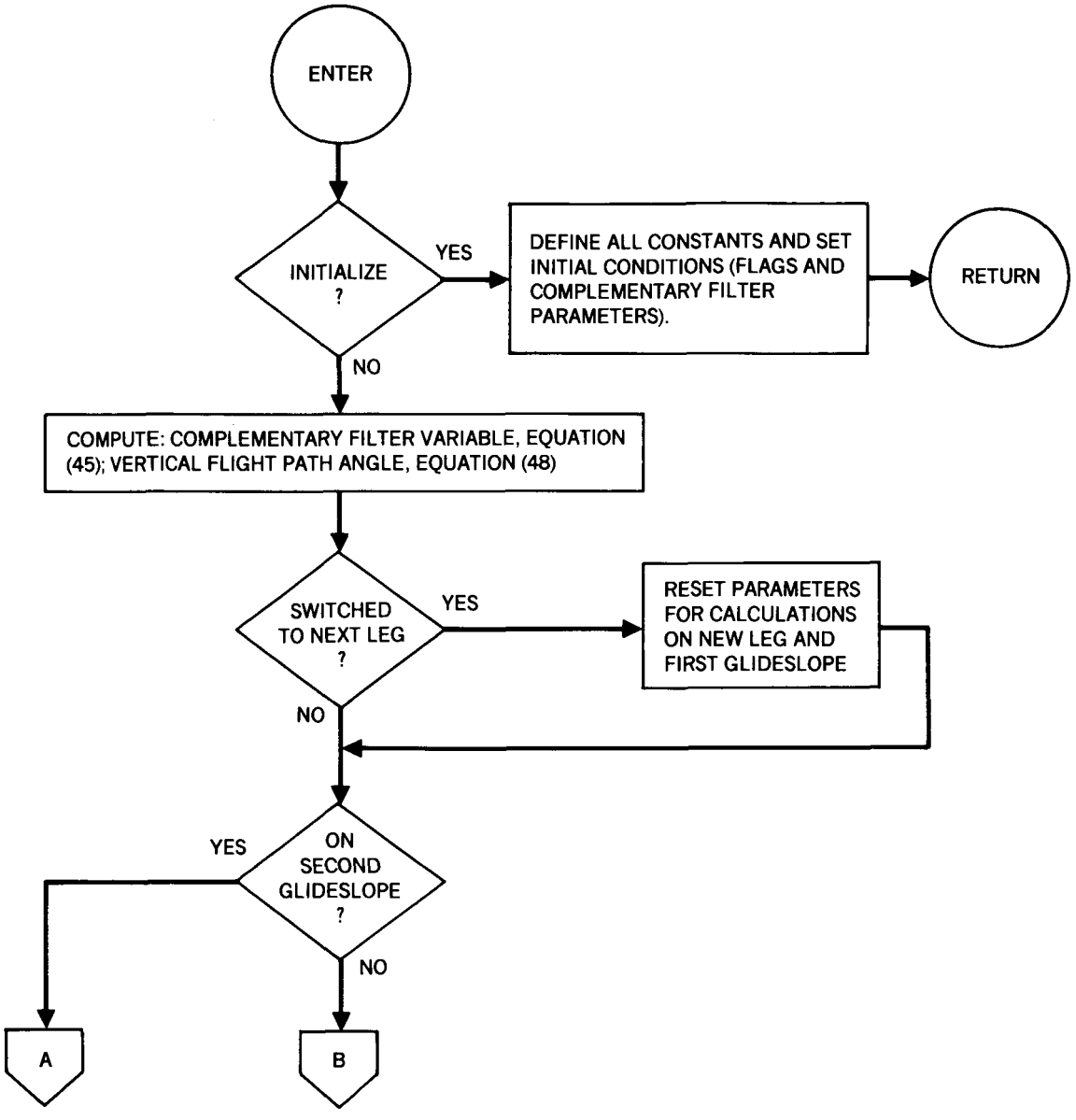

Figure 15. Vertical Guidance Flow Diagram (Sheet 1)

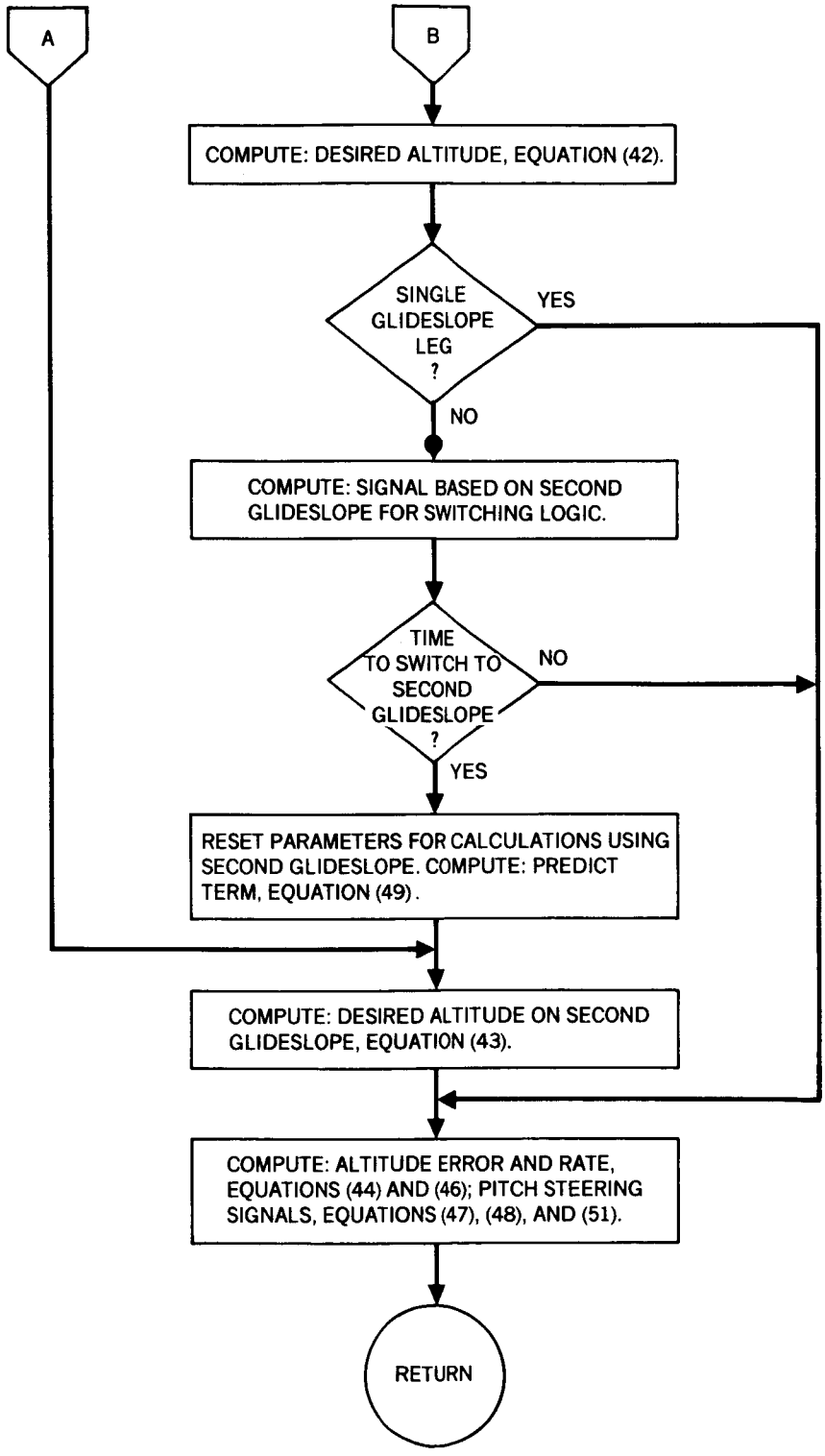

Figure 15. Vertical Guidance Flow Diagram (Sheet 2)

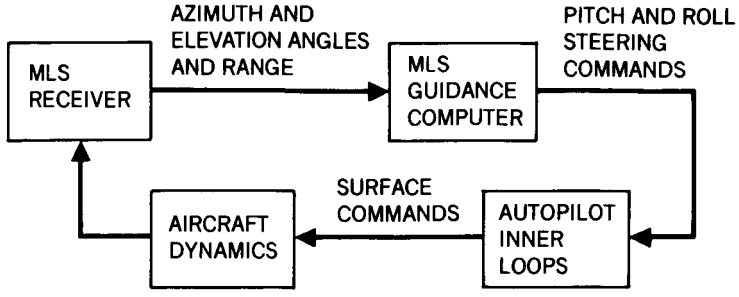

Figure 16. Block Diagram of MLS Pitch and Roll Guidance Systems

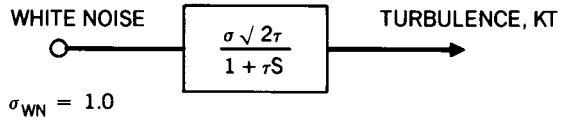

FILTER PARAMETERS

	LONGITUDINAL	LATERAL	VERTICAL
τ(SEC)	$600/V_{TAS}$	$600/V_{TAS}$	$30/V_{TAS}$
σ(KT)	$0.15\,\lvert W_x \rvert$	$0.15\,\lvert W_y \rvert$	1.5

Figure 17. Turbulence Model Used in Simulation

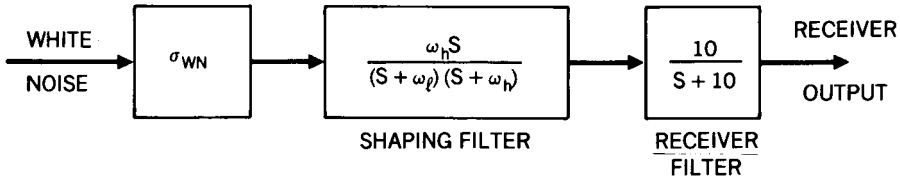

AZIMUTH	ELEVATION	DME
ω_ℓ = 0.001 RAD/SEC	ω_ℓ = 0.001 RAD/SEC	ω_ℓ = 0.001 RAD/SEC
ω_h = 0.16 RAD/SEC	ω_h = 0.34 RAD/SEC	ω_h = 0.245 RAD/SEC
σ_{WN} = 0.064	σ_{WN} = 0.024	σ_{WN} = 154.7
σ_{REC} = 0.02 DEG	σ_{REC} = 0.0097 DEG	σ_{REC} = 53.4 FT

Figure 18. MLS Noise Model Used in Simulation (1σ or 68-Percent Probability)

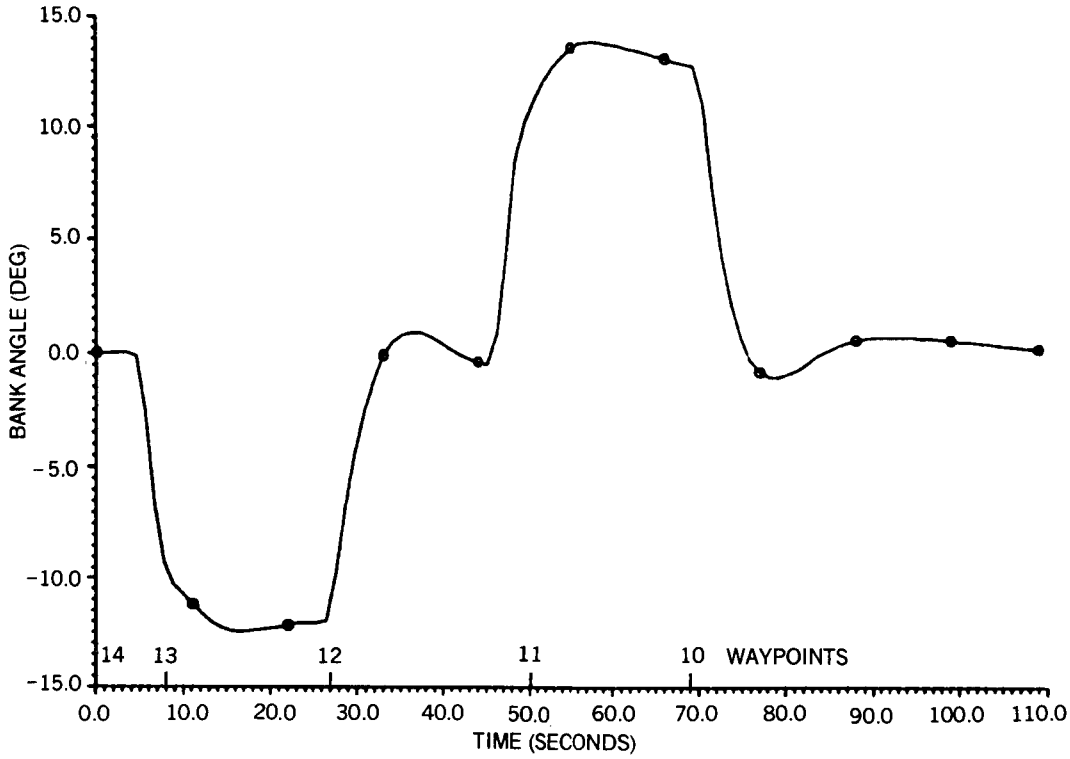

Figure 19. Bank Angle, Case 1 (Initial Approach, Baseline)

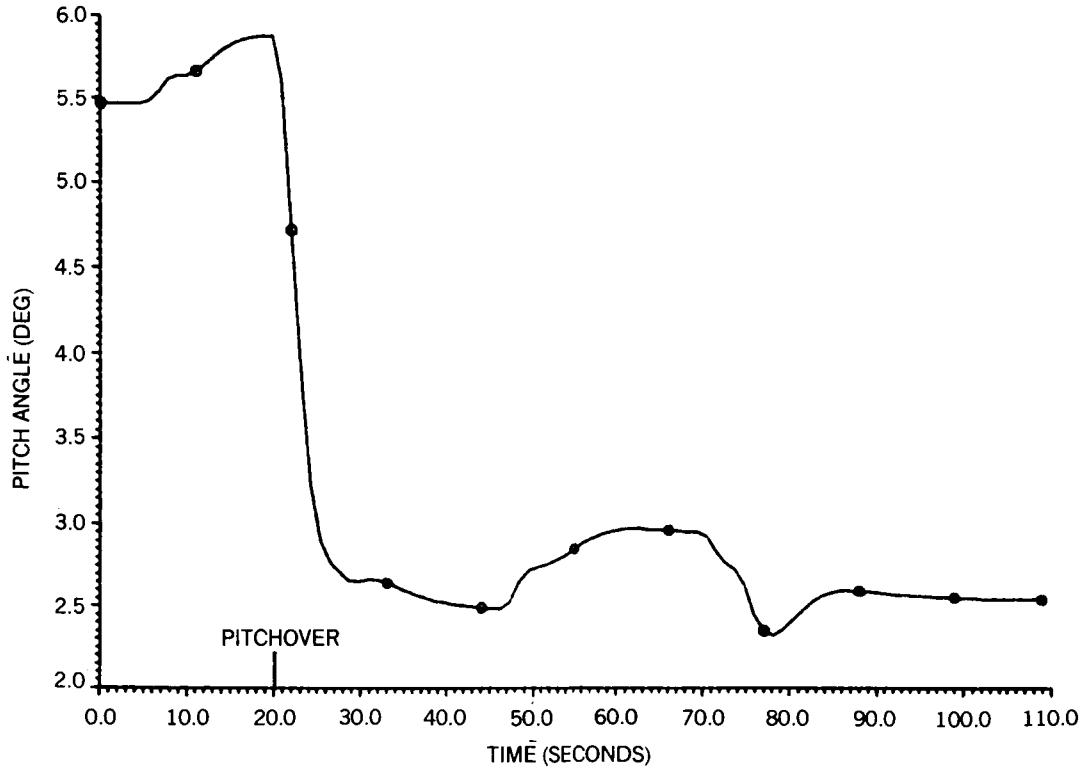

Figure 20. Pitch Angle, Case 1 (Initial Approach, Baseline)

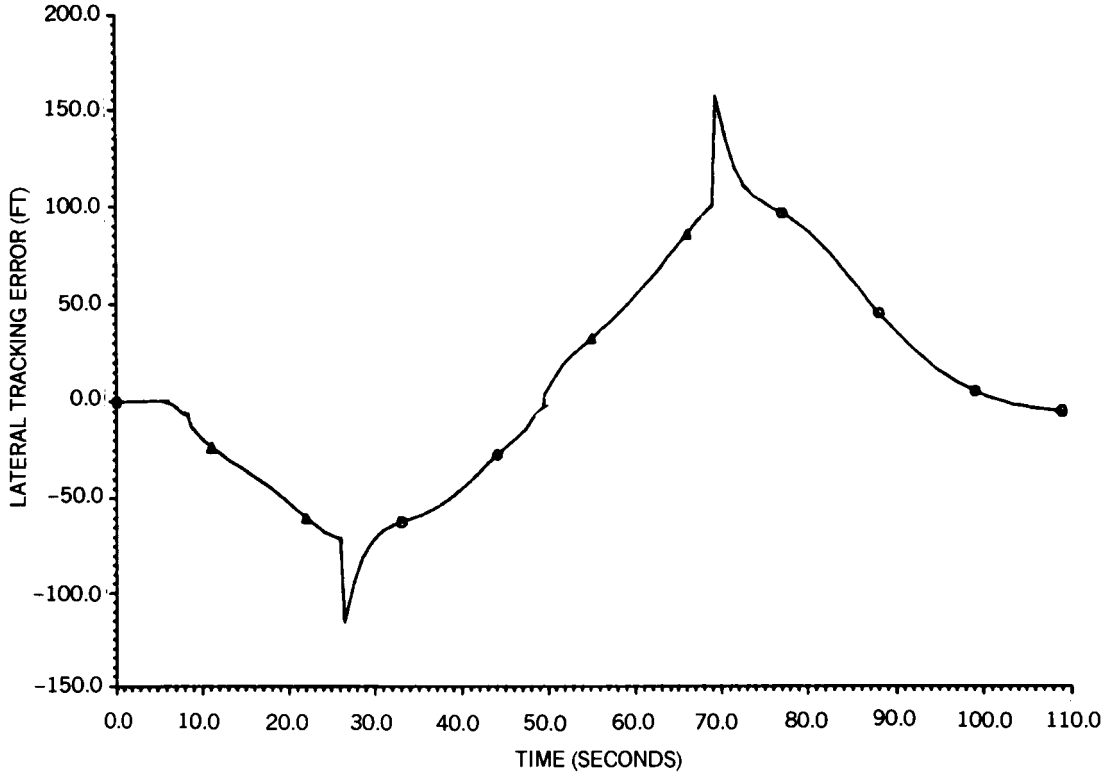

Figure 21. Lateral Tracking Error, Case 1 (Initial Approach, Baseline)

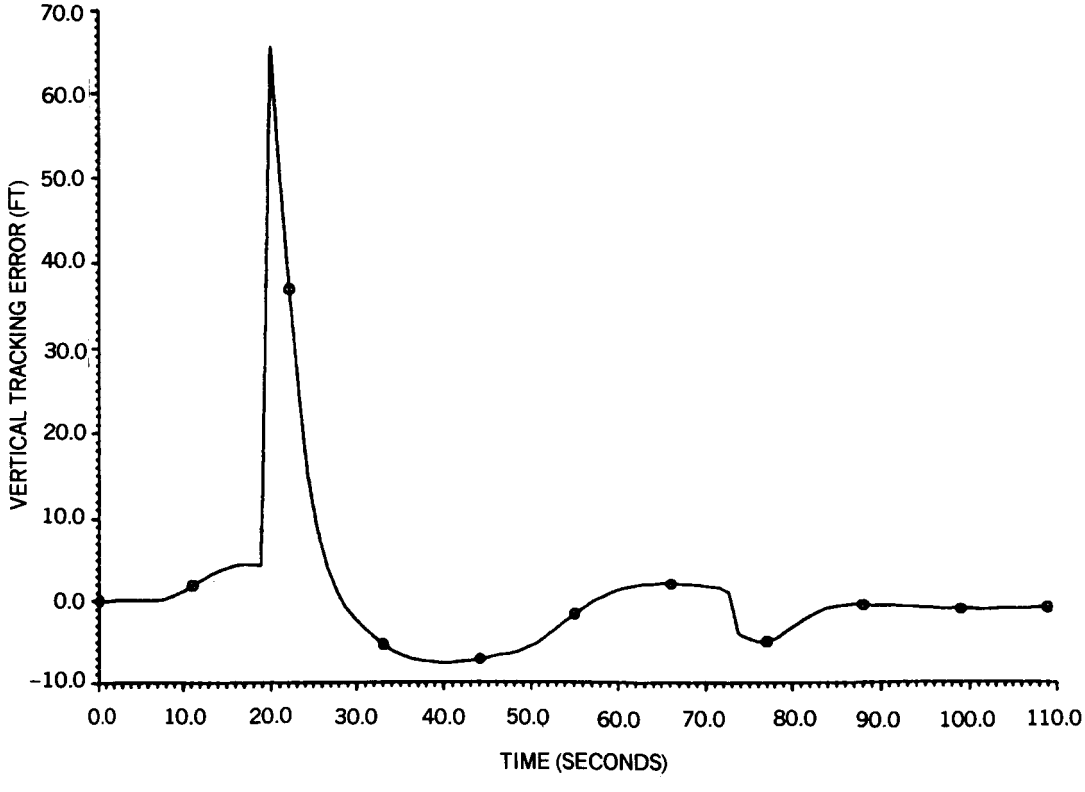

Figure 22. Vertical Tracking Error, Case 1 (Initial Approach Baseline)

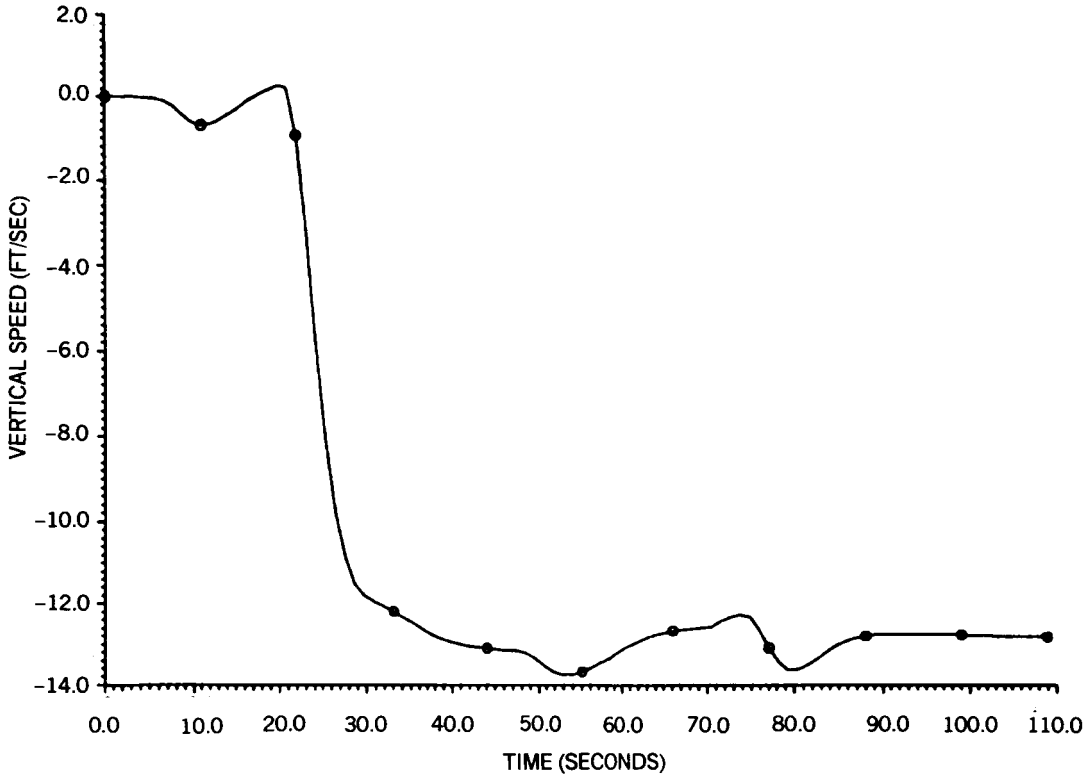

Figure 23. Vertical Speed, Case 1 (Initial Approach Baseline)

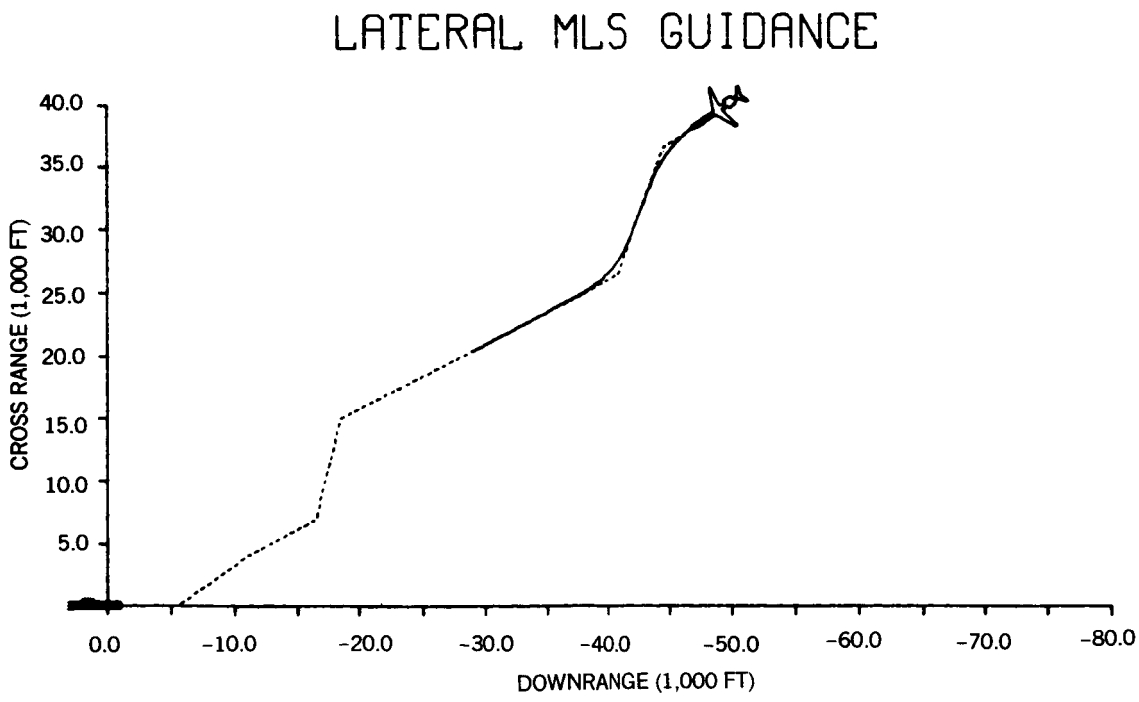

Figure 24. Ground Track, Case 1 (Initial Approach Baseline)

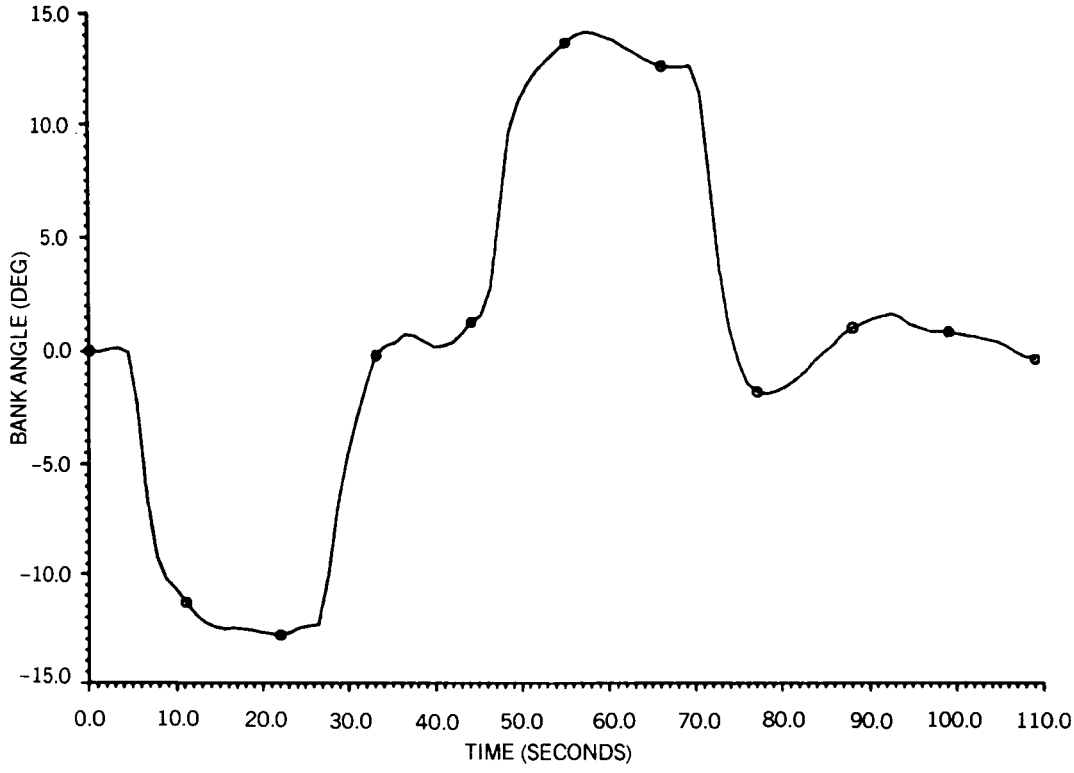

Figure 25. Bank Angle, Case 2 (Initial Approach, MLS Noise)

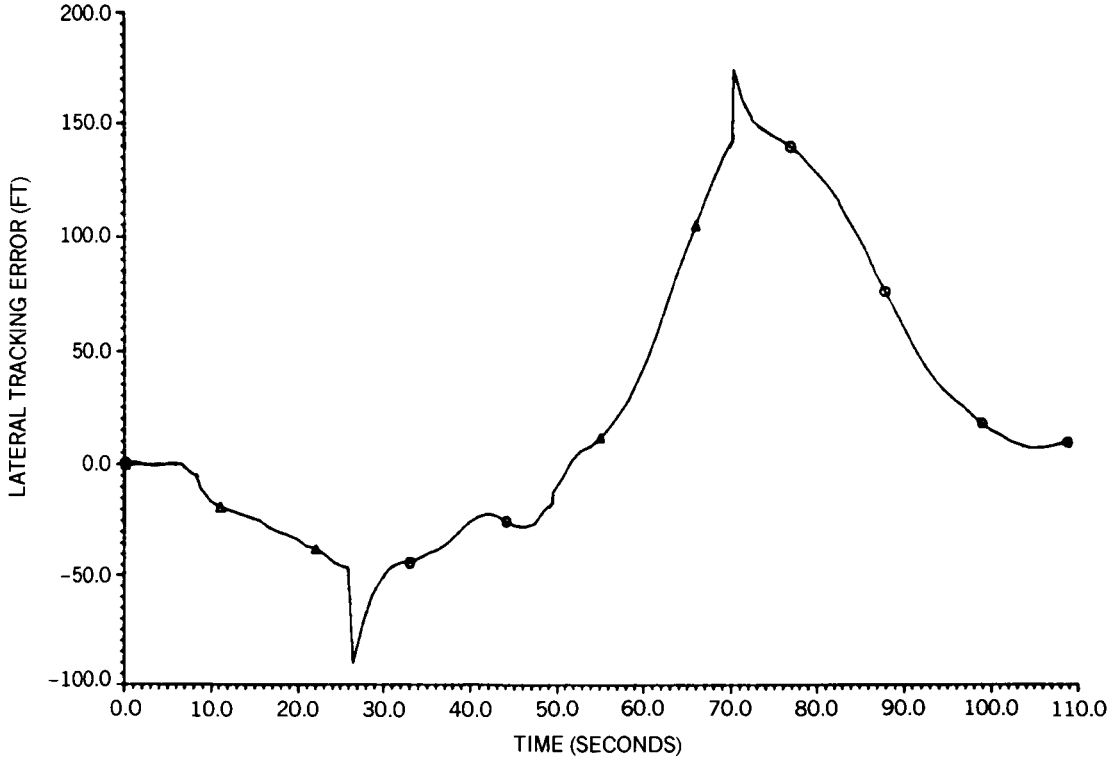

Figure 26. Lateral Tracking Error, Case 2 (Initial Approach, MLS Noise)

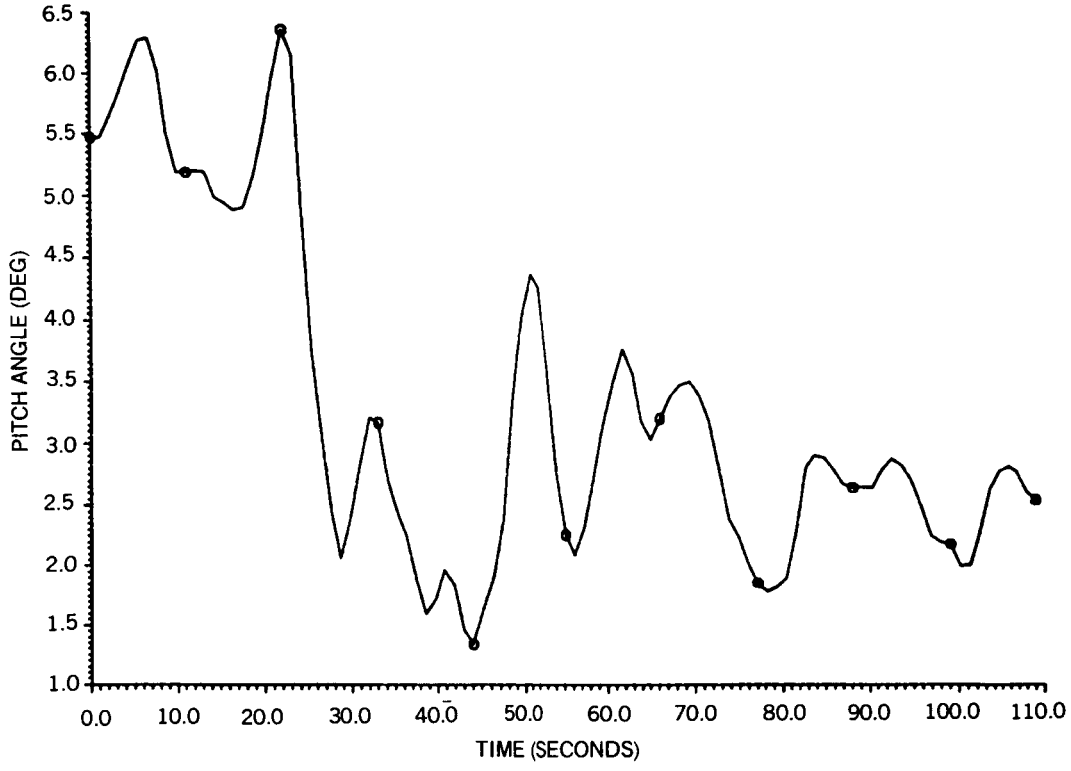

Figure 27. Pitch Angle, Case 2 (Initial Approach, MLS Noise)

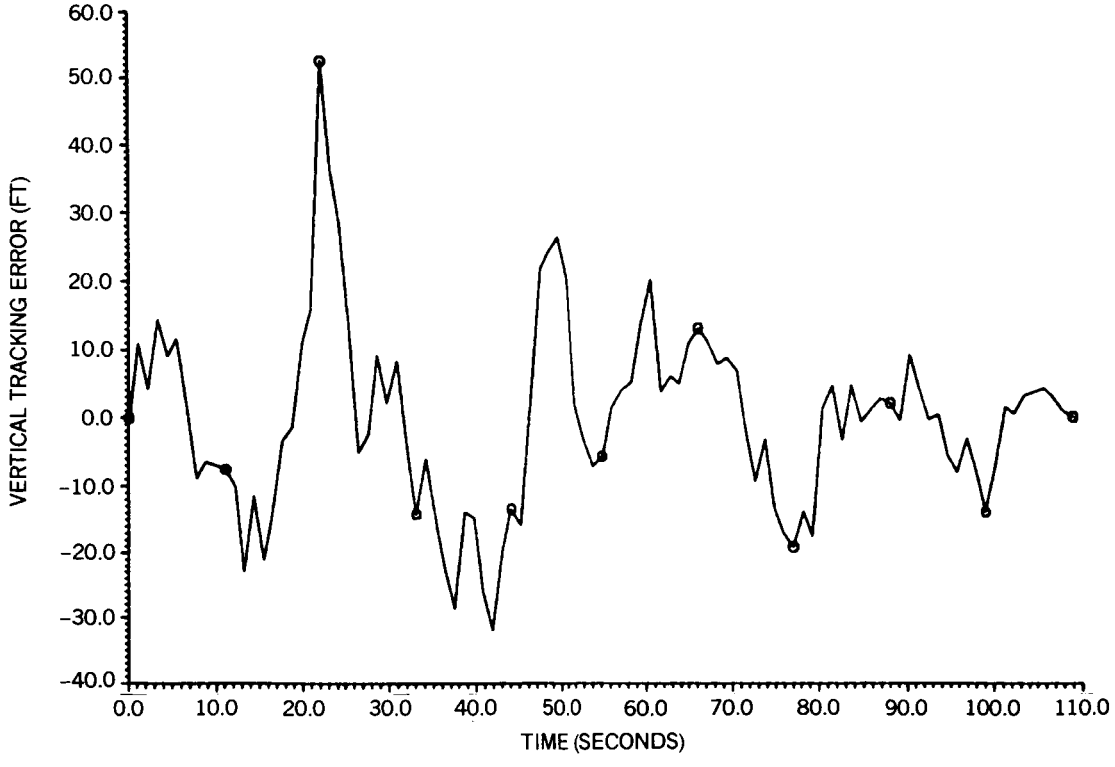

Figure 28. Vertical Tracking Error, Case 2 (Initial Approach, MLS Noise)

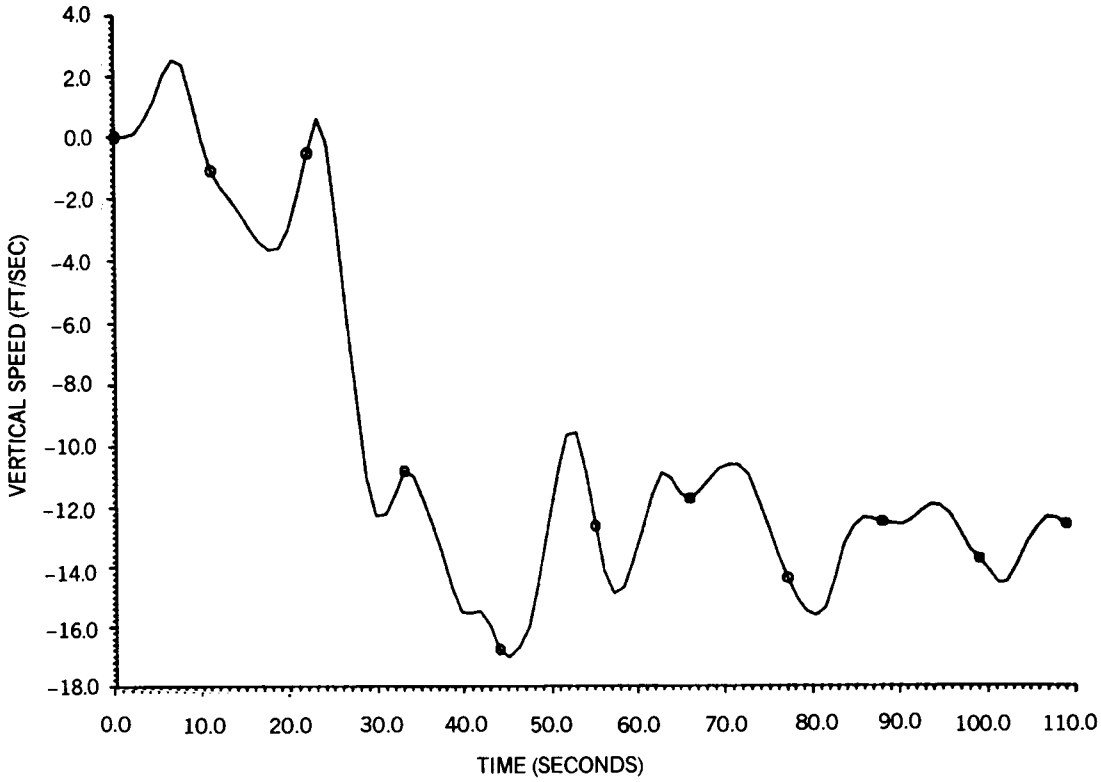

Figure 29. Vertical Speed, Case 2 (Initial Approach, MLS Noise)

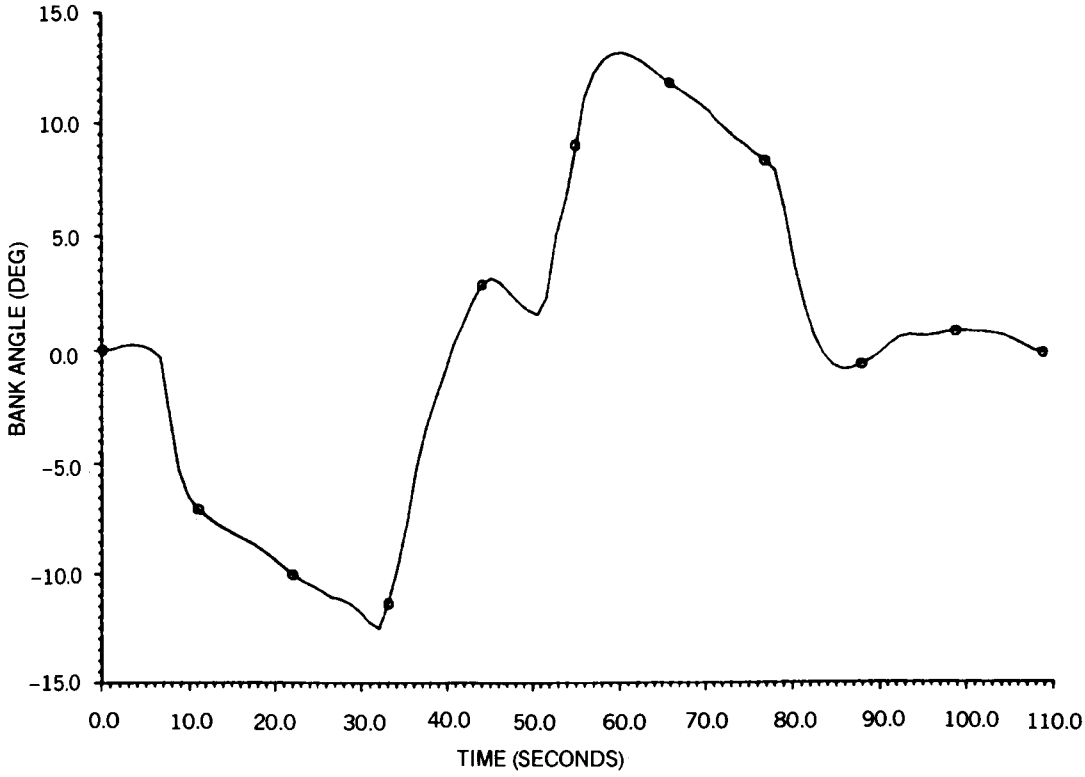

Figure 30. Bank Angle, Case 3 (Initial Approach, Wind)

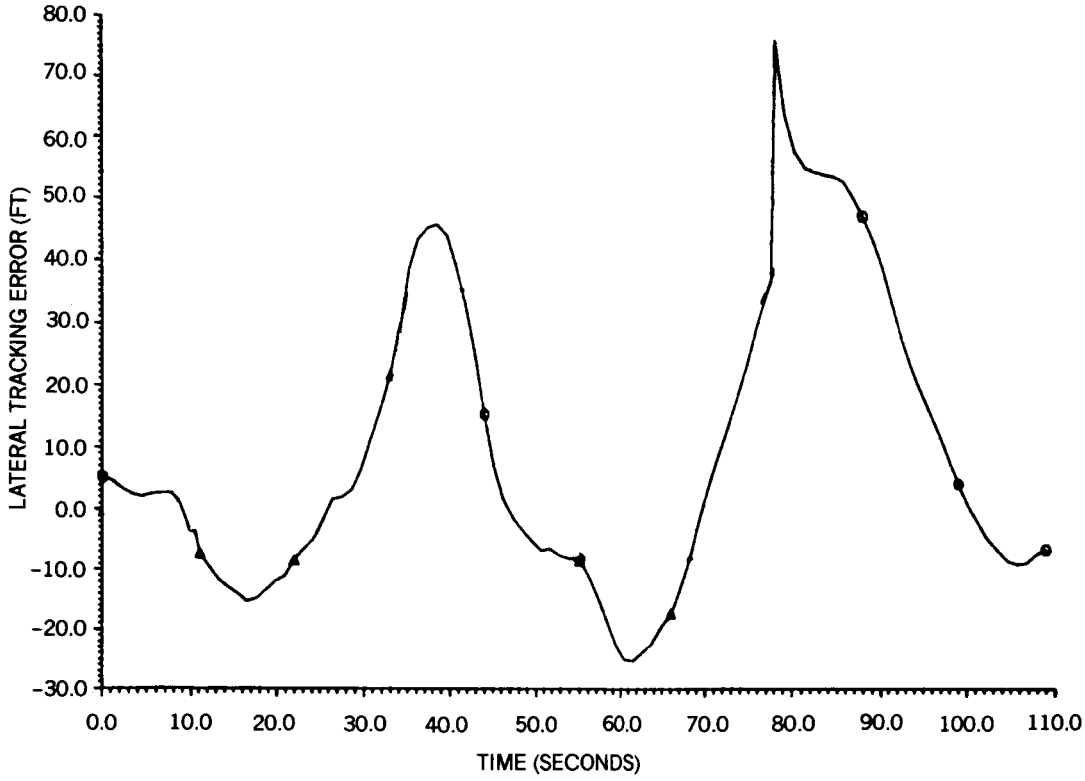

Figure 31. Lateral Tracking Error, Case 3 (Initial Approach, Wind)

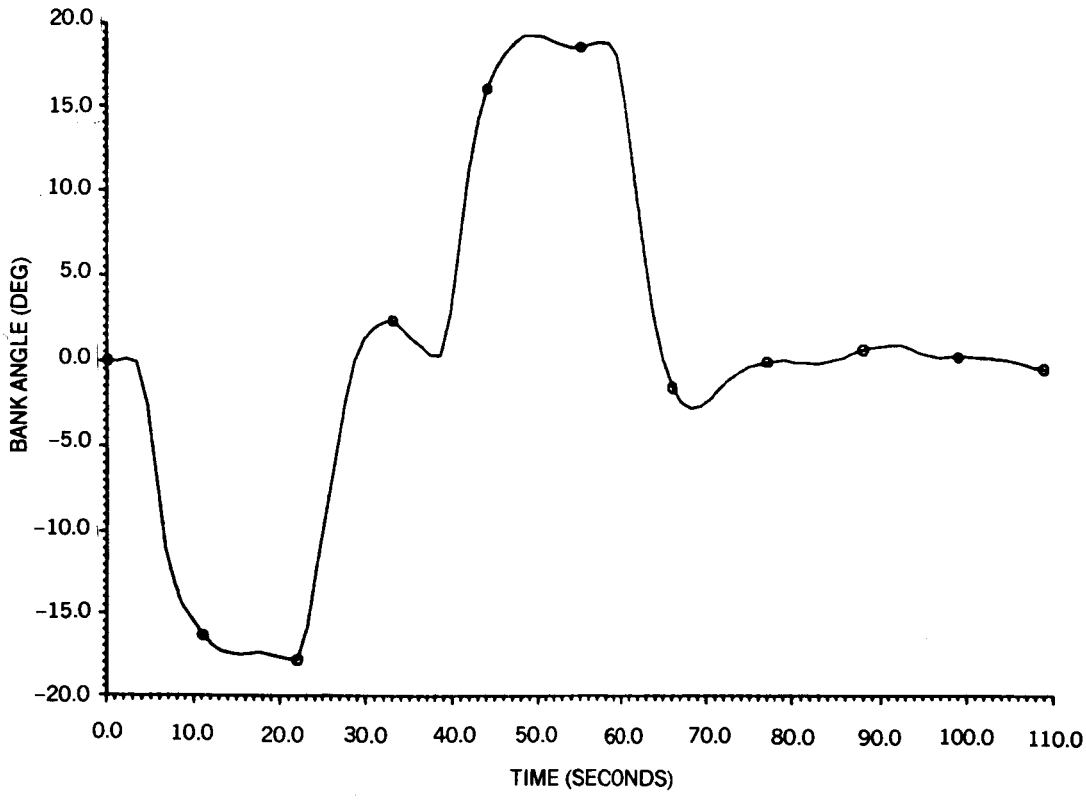

Figure 32. Bank Angle, Case 4 (Initial Approach, Speed Change)

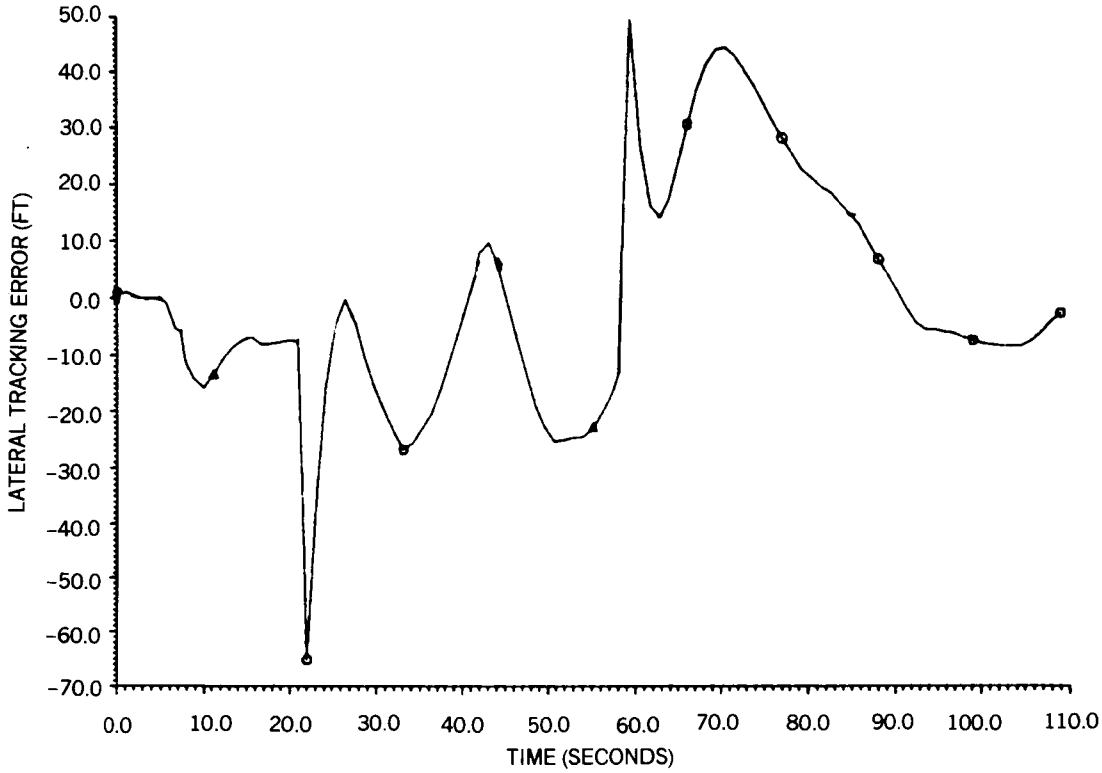

Figure 33. Lateral Tracking Error, Case 4 (Initial Approach, Speed Change)

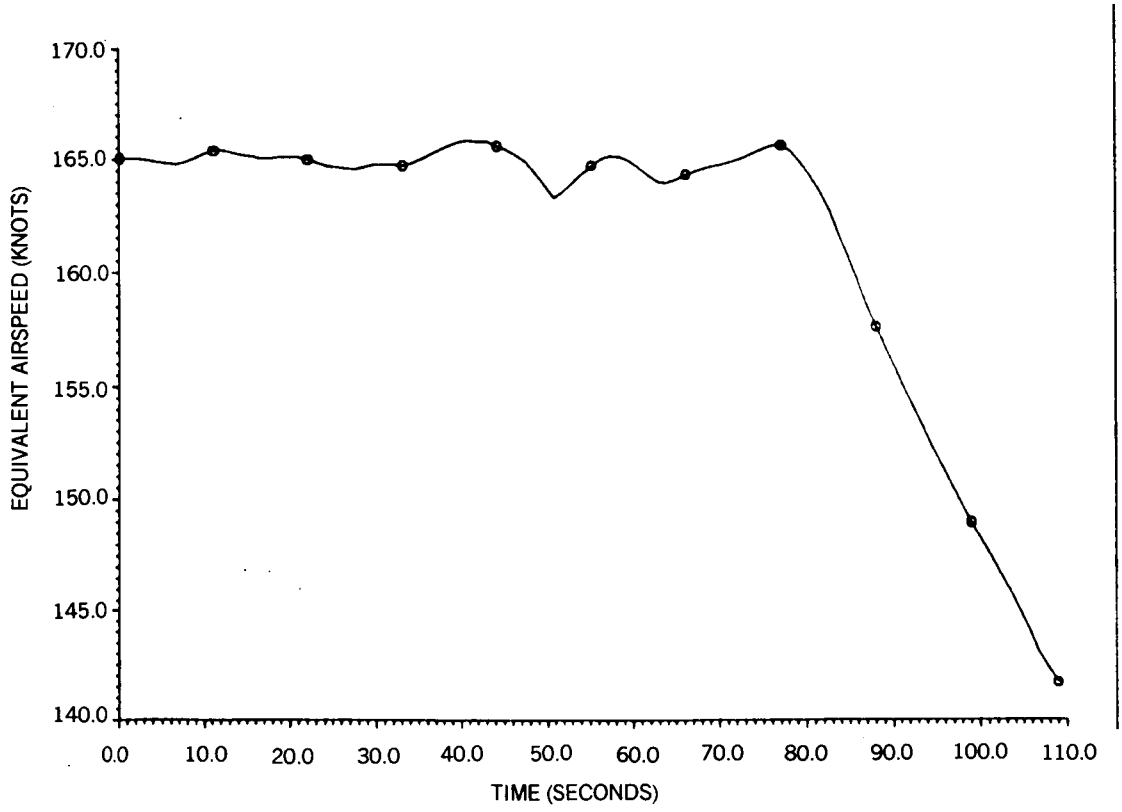

Figure 34. Airspeed, Case 4 (Initial Approach, Speed Change)

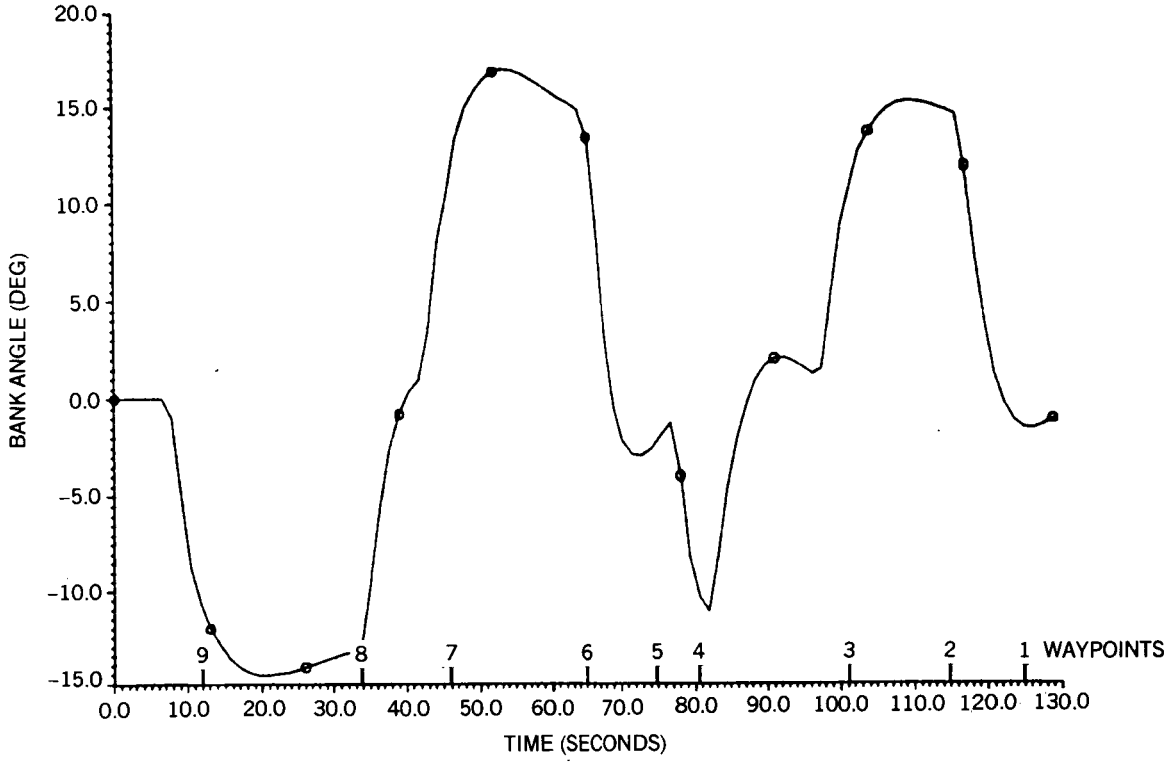

Figure 35. Bank Angle, Case 5 (Final Approach, Baseline)

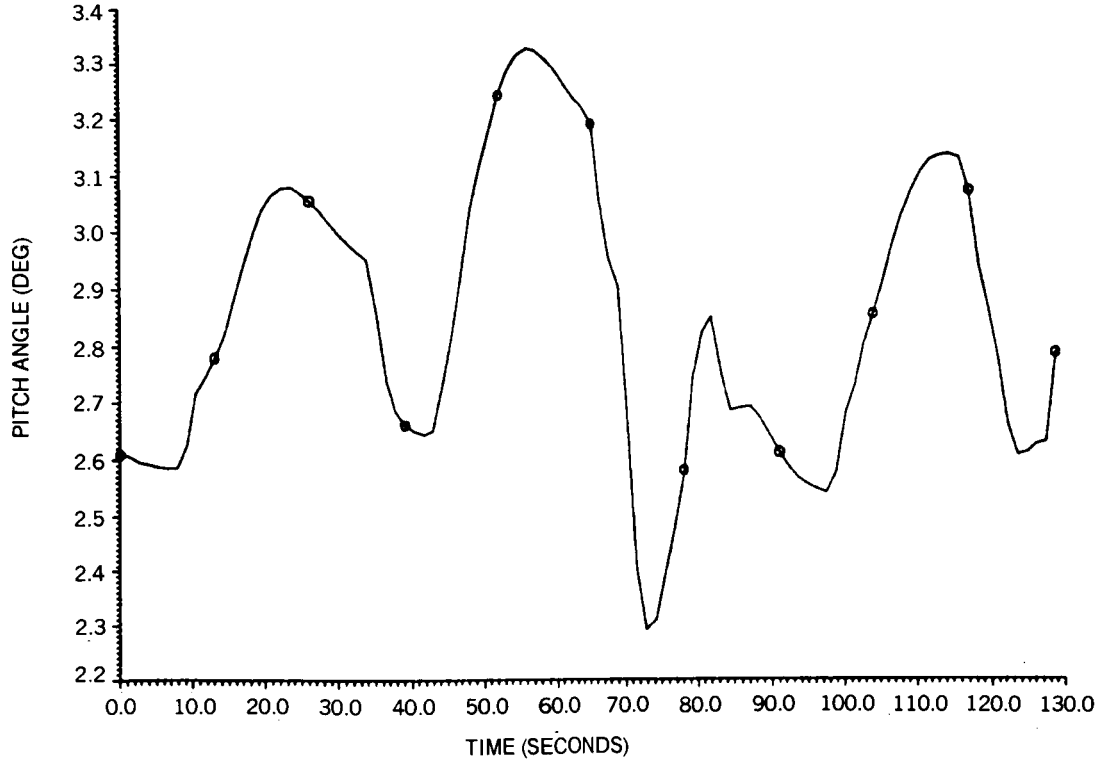

Figure 36. Pitch Angle, Case 5 (Final Approach, Baseline)

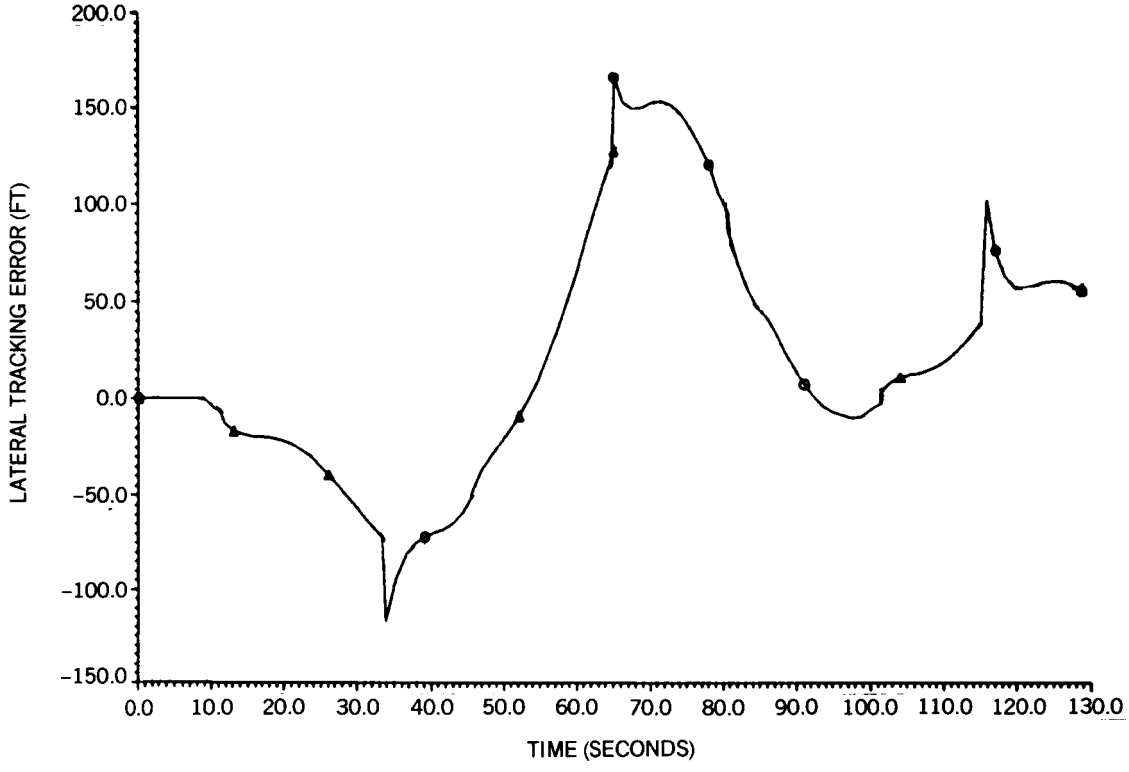

Figure 37. Lateral Tracking Error, Case 5 (Final Approach, Baseline)

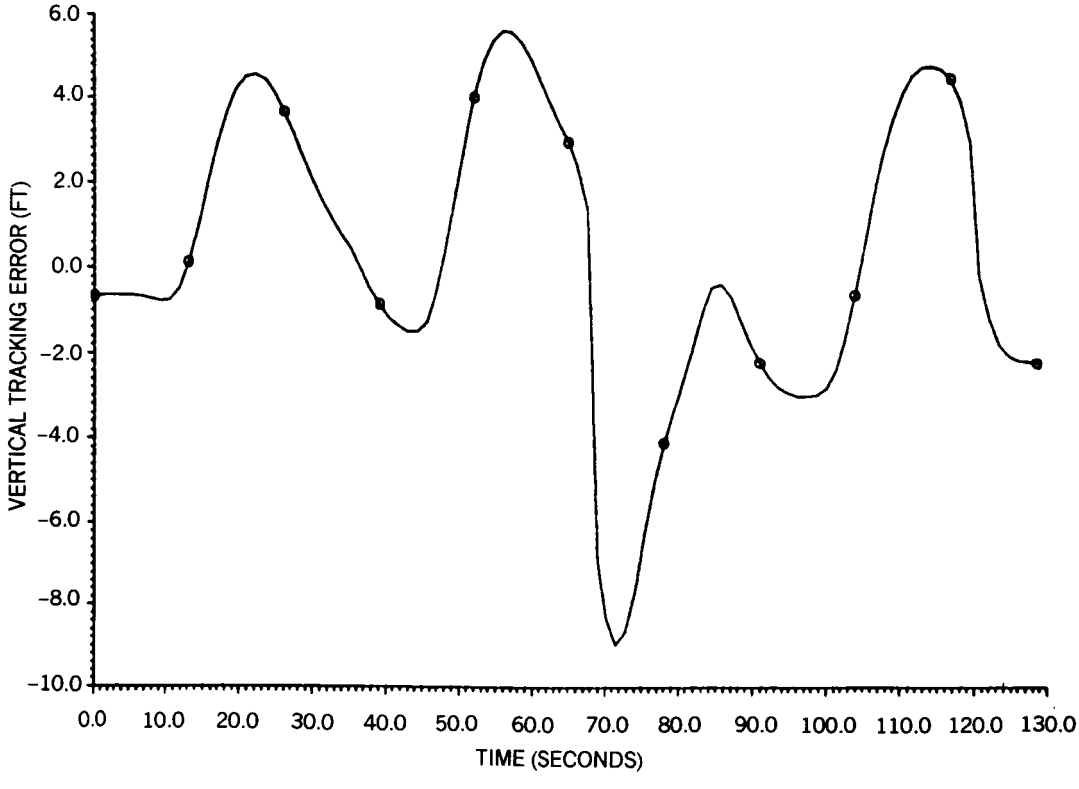

Figure 38. Vertical Tracking Error, Case 5 (Final Approach, Baseline)

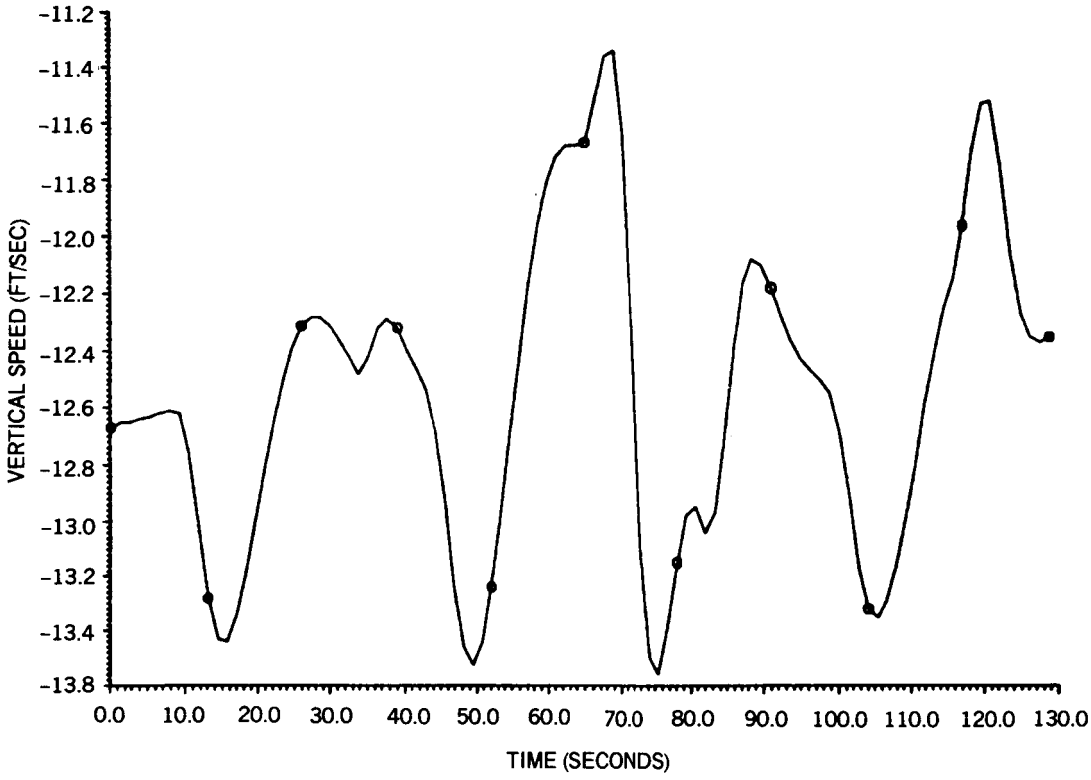

Figure 39. Vertical Speed, Case 5 (Final Approach, Baseline)

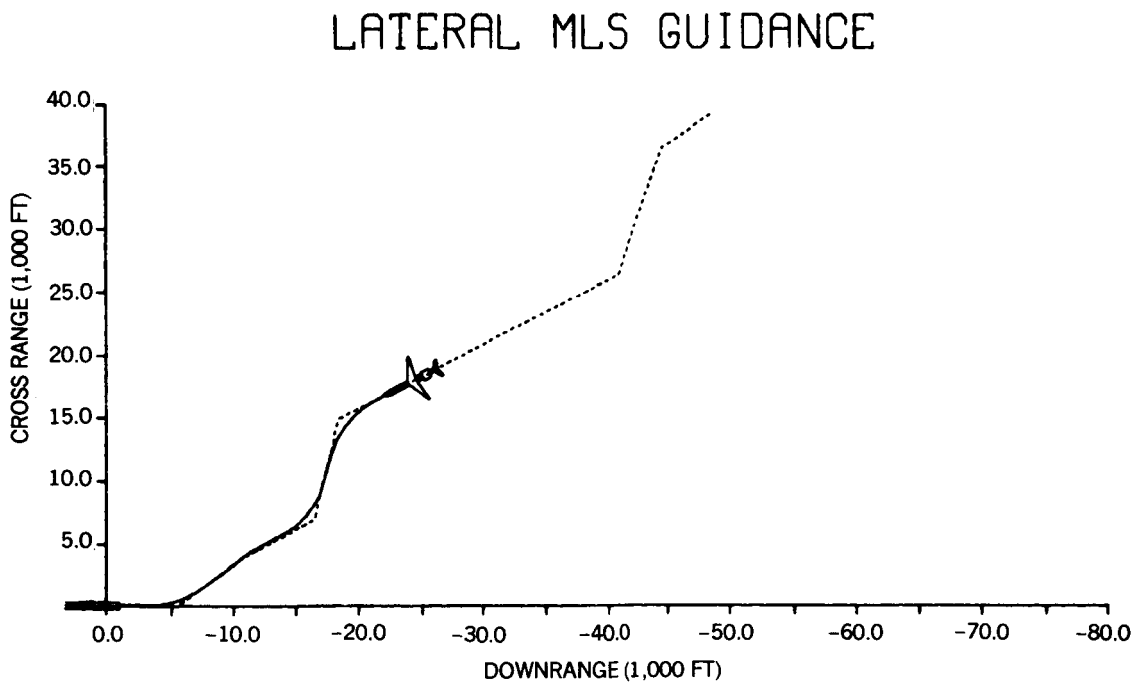

Figure 40. Ground Track, Case 5 (Final Approach, Baseline)

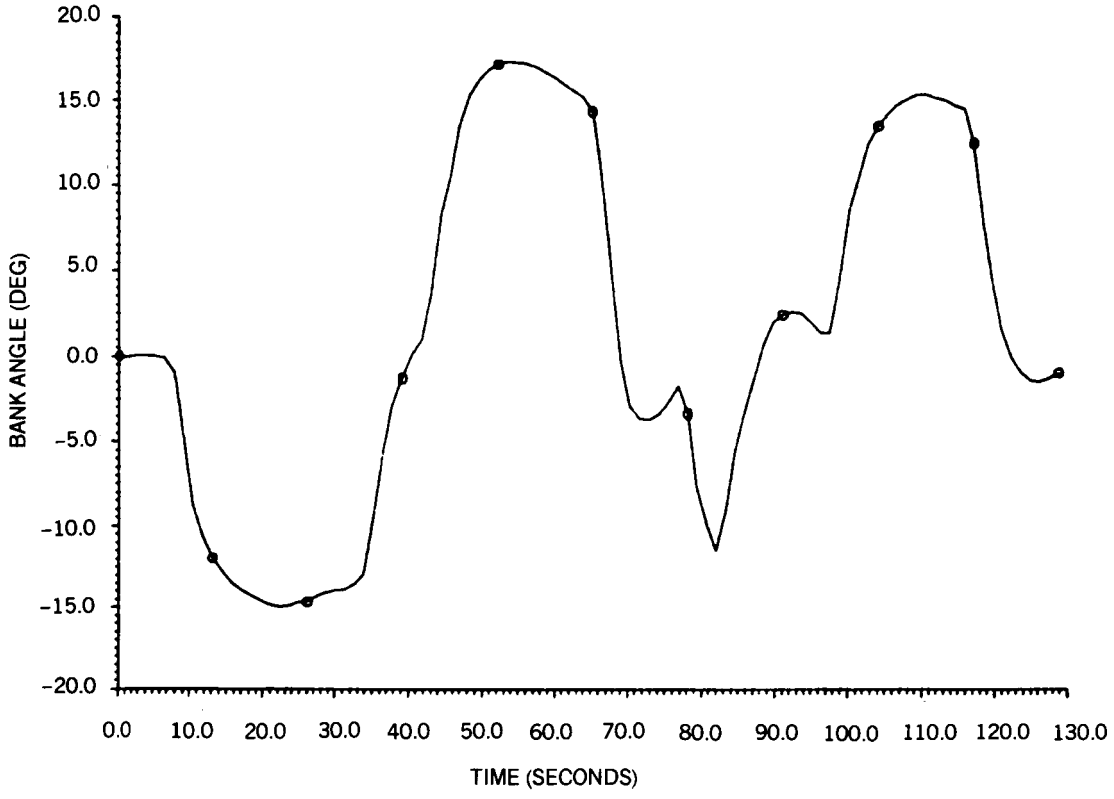

Figure 41. Bank Angle, Case 6 (Final Approach, MLS Noise)

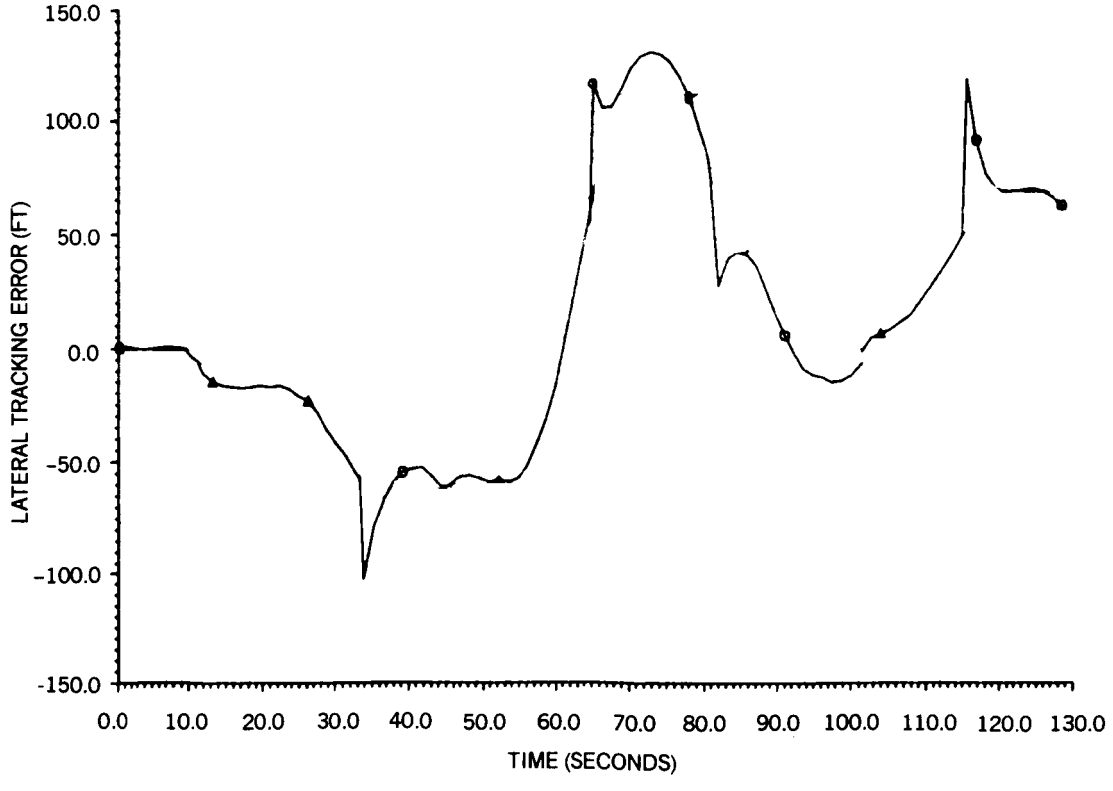

Figure 42. Lateral Tracking Error, Case 6 (Final Approach, MLS Noise)

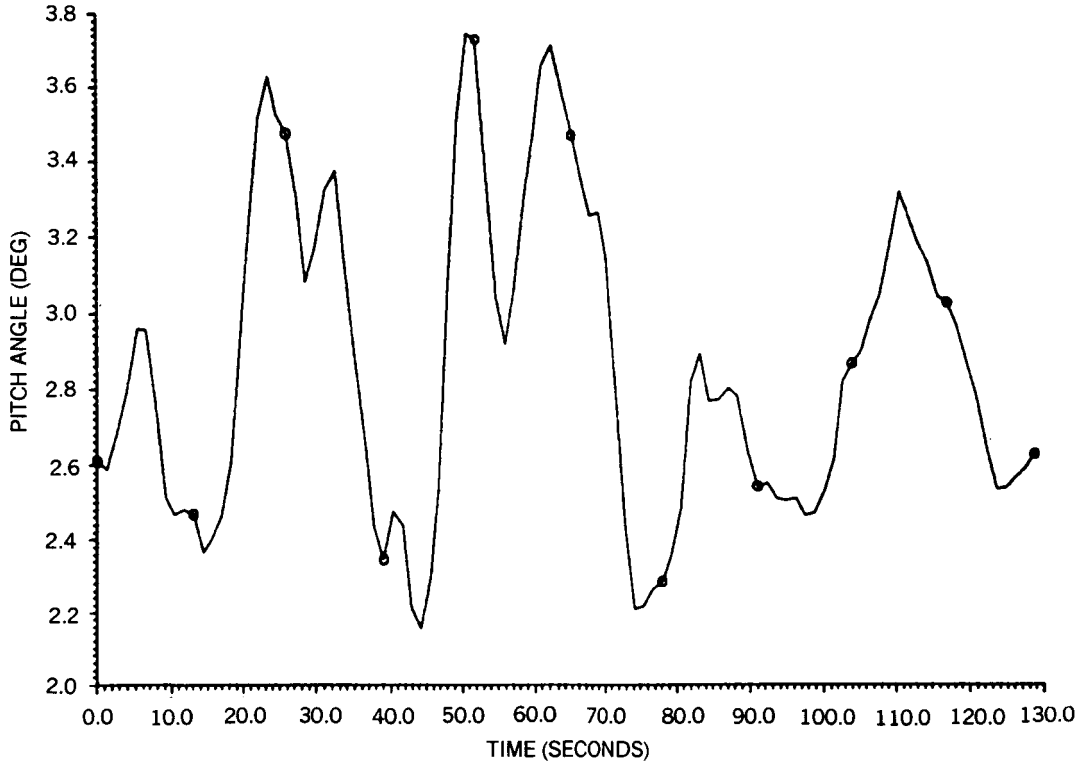

Figure 43. Pitch Angle, Case 6 (Final Approach, MLS Noise)

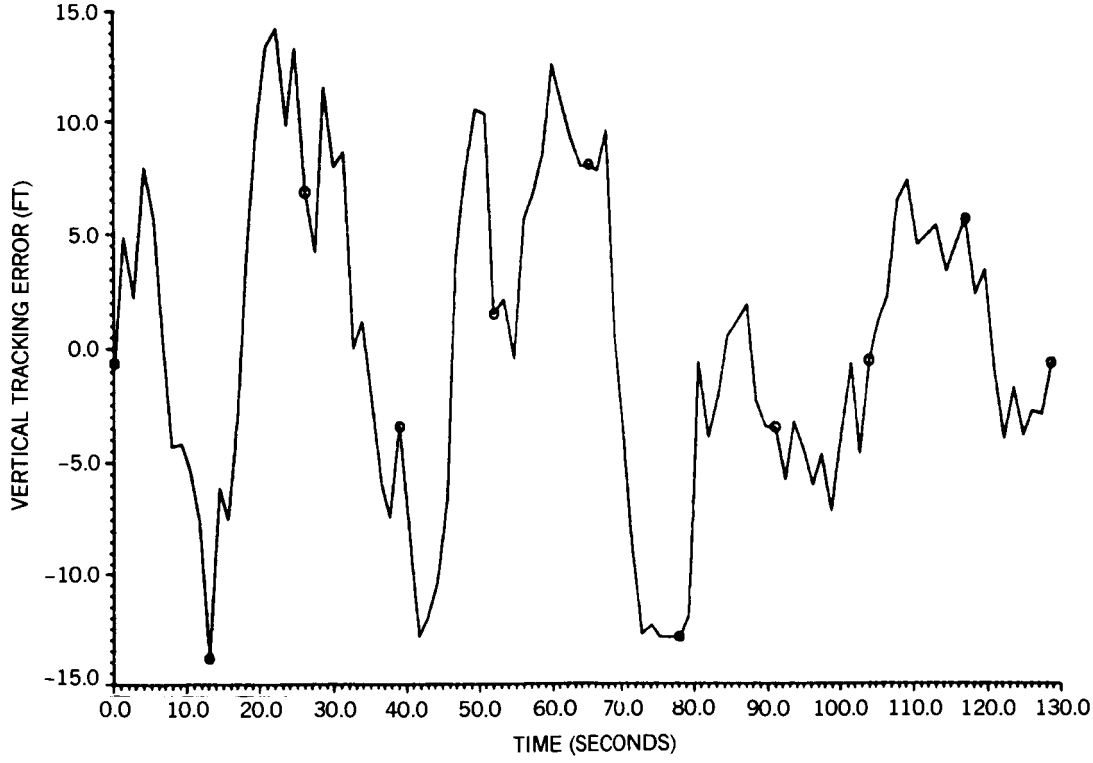

Figure 44. Vertical Tracking Error, Case 6 (Final Approach, MLS Noise)

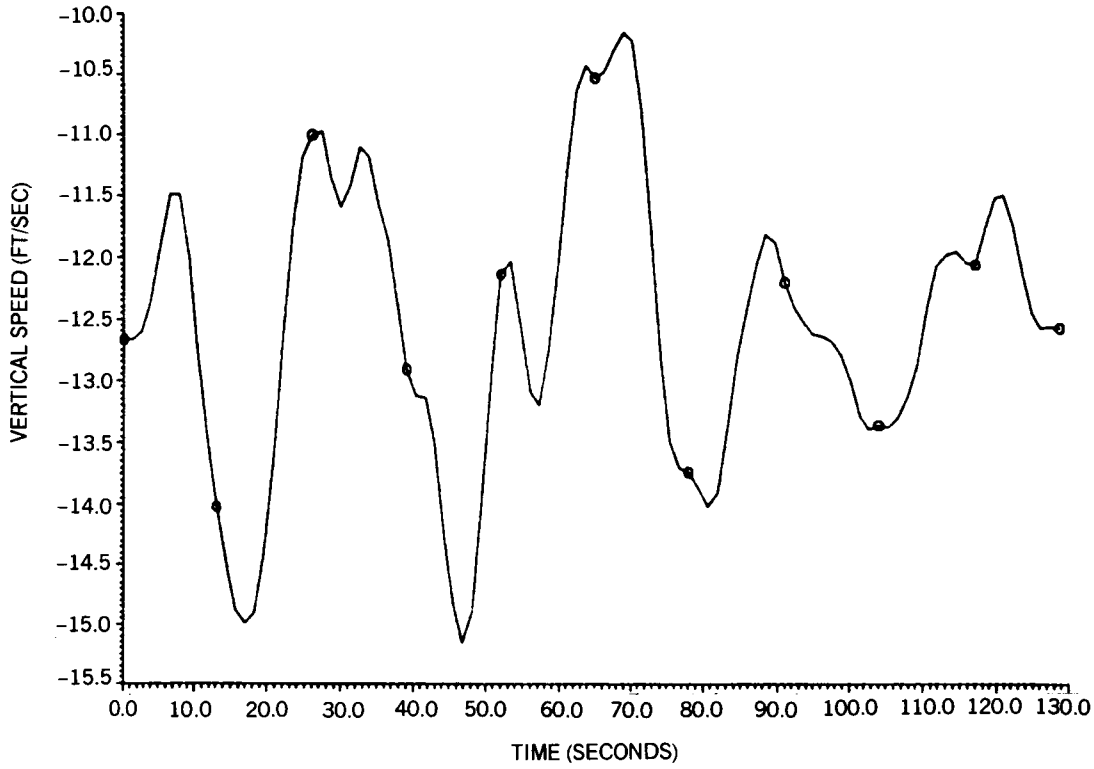

Figure 45. Vertical Speed, Case 6 (Final Approach, MLS Noise)

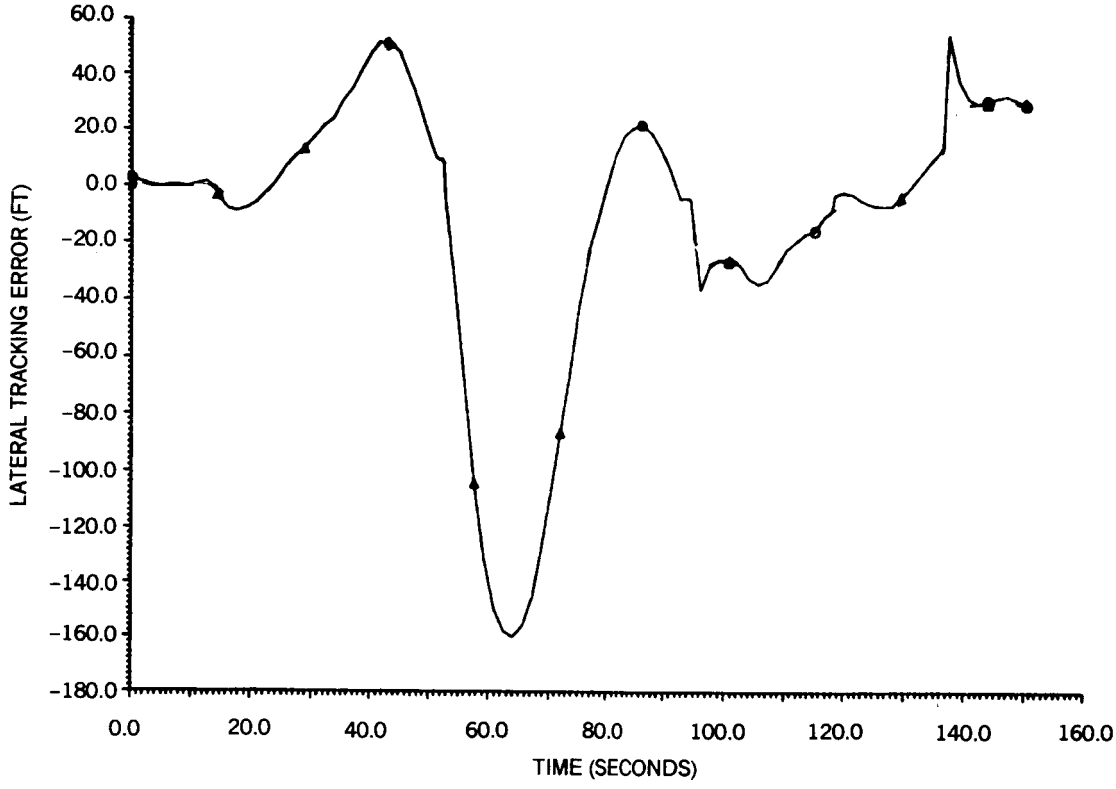

Figure 46(A). Lateral Tracking Error, Case 7 (Final Approach, Wind)

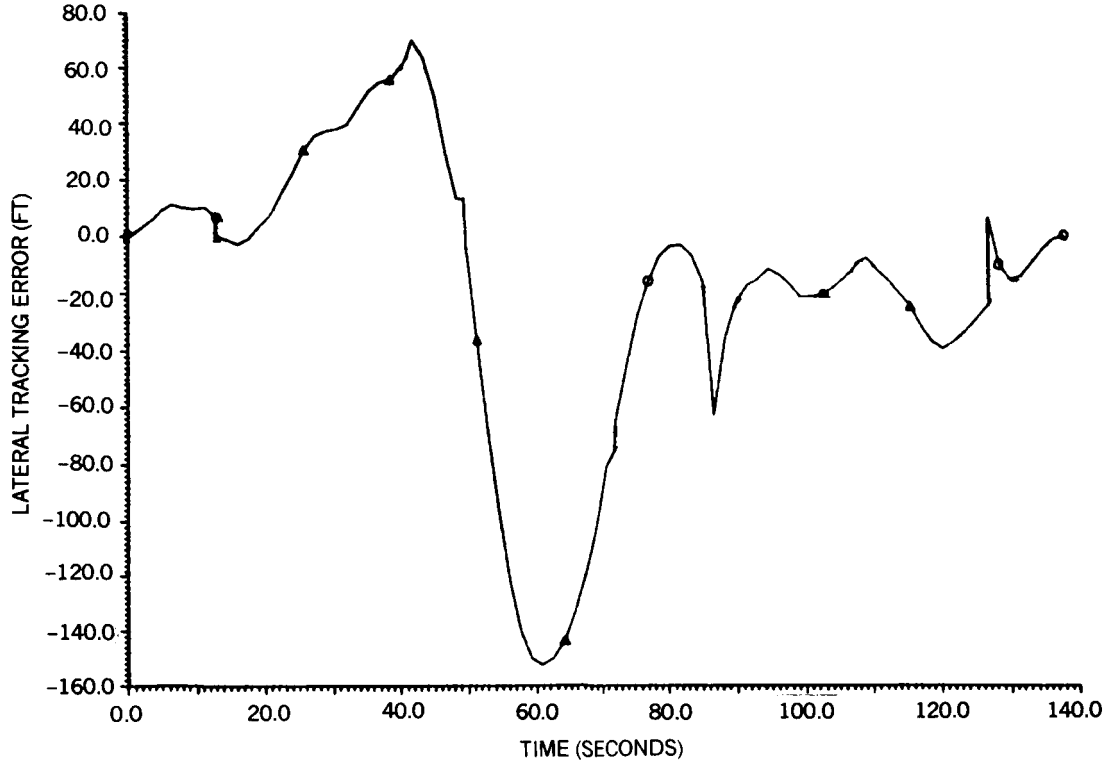

Figure 46(B). Lateral Tracking Error, Case 8 (Final Approach, Turbulence)

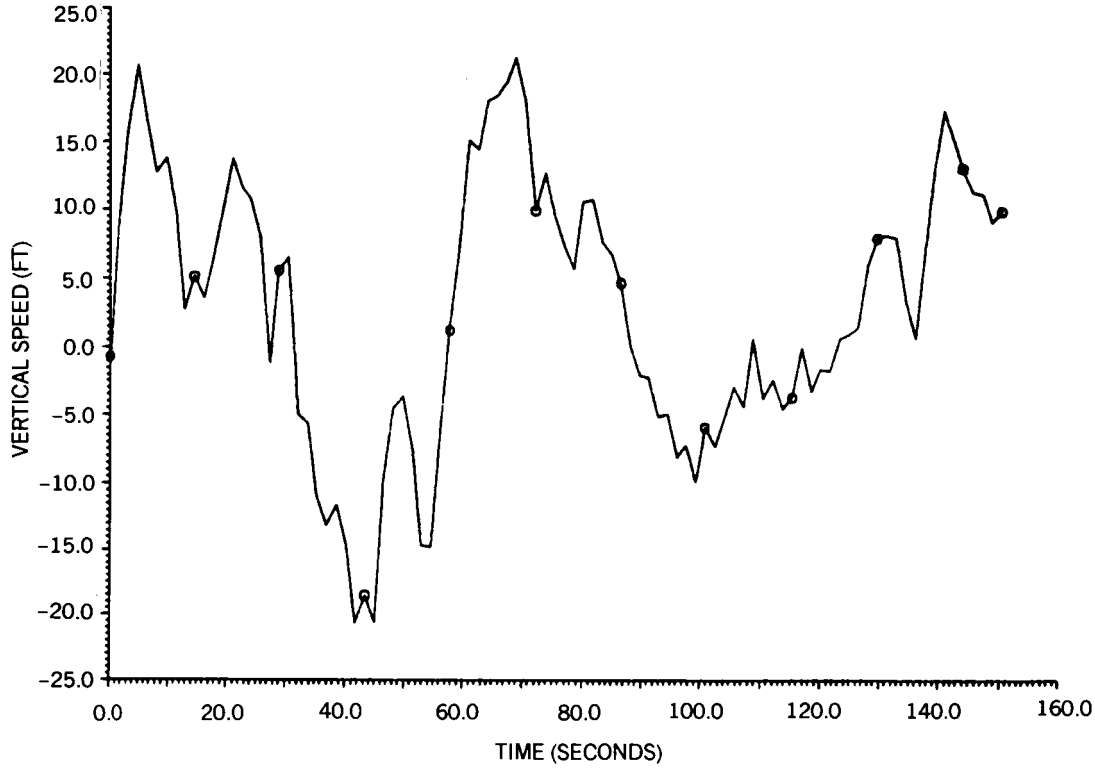

Figure 47(A). Vertical Tracking Error, Case 7 (Final Approach, Turbluence)

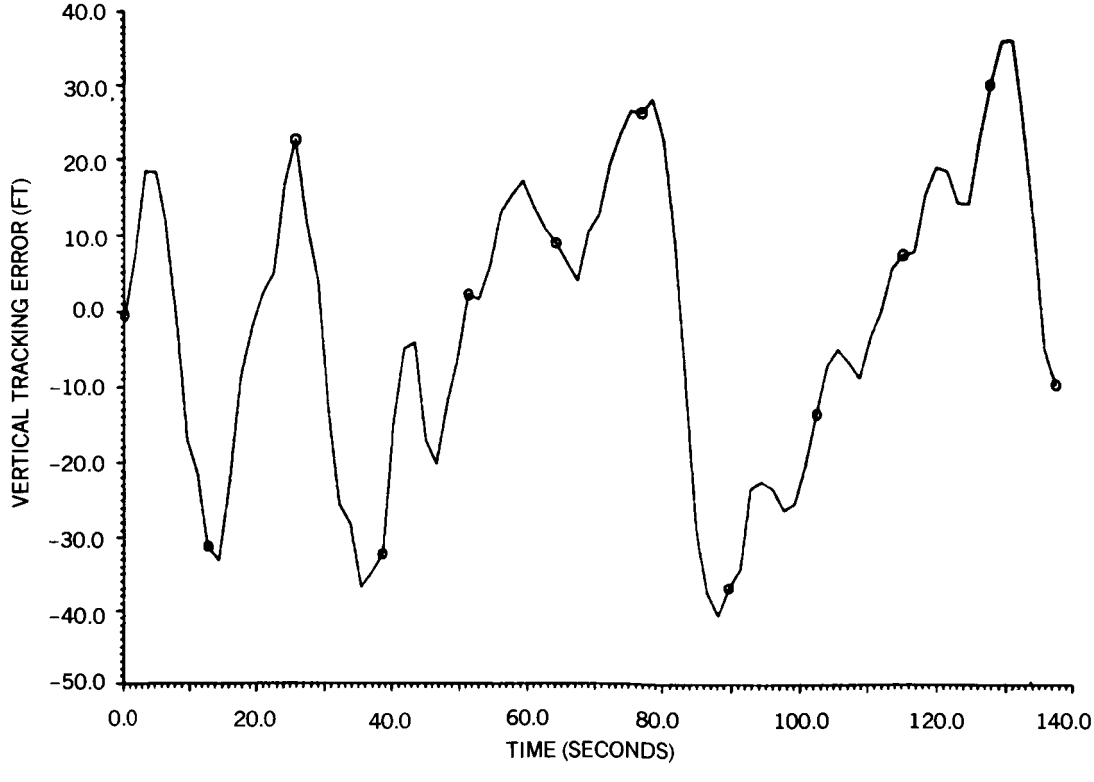

Figure 47(B). Vertical Tracking Error, Case 8 (Final Approach, Turbulence)

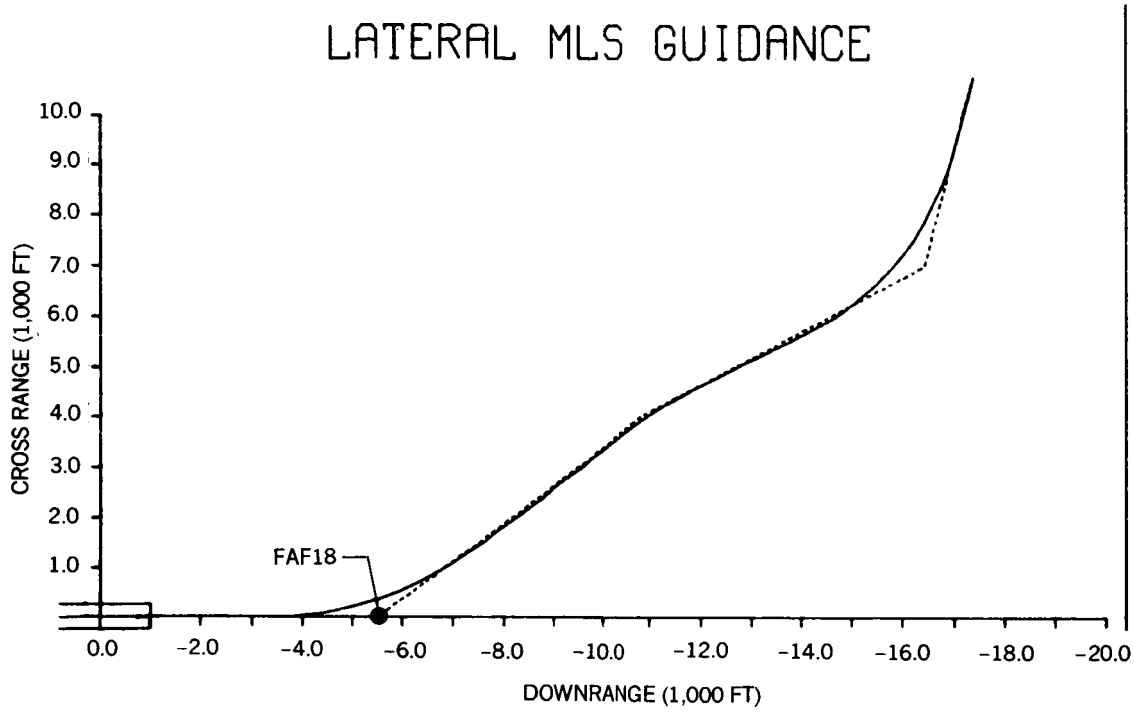

Figure 48. Ground Track, Case 8 (Final Approach, Turbulence)

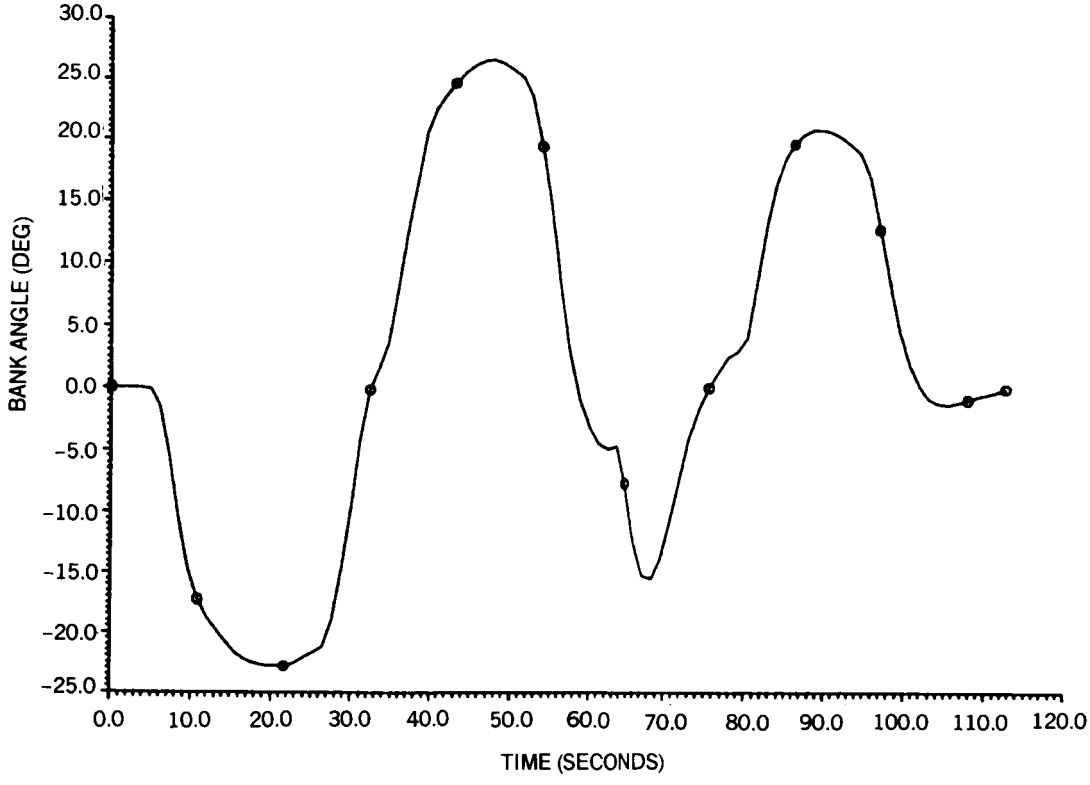

Figure 49. Bank Angle, Case 9 (Final Approach, Wind Shear)

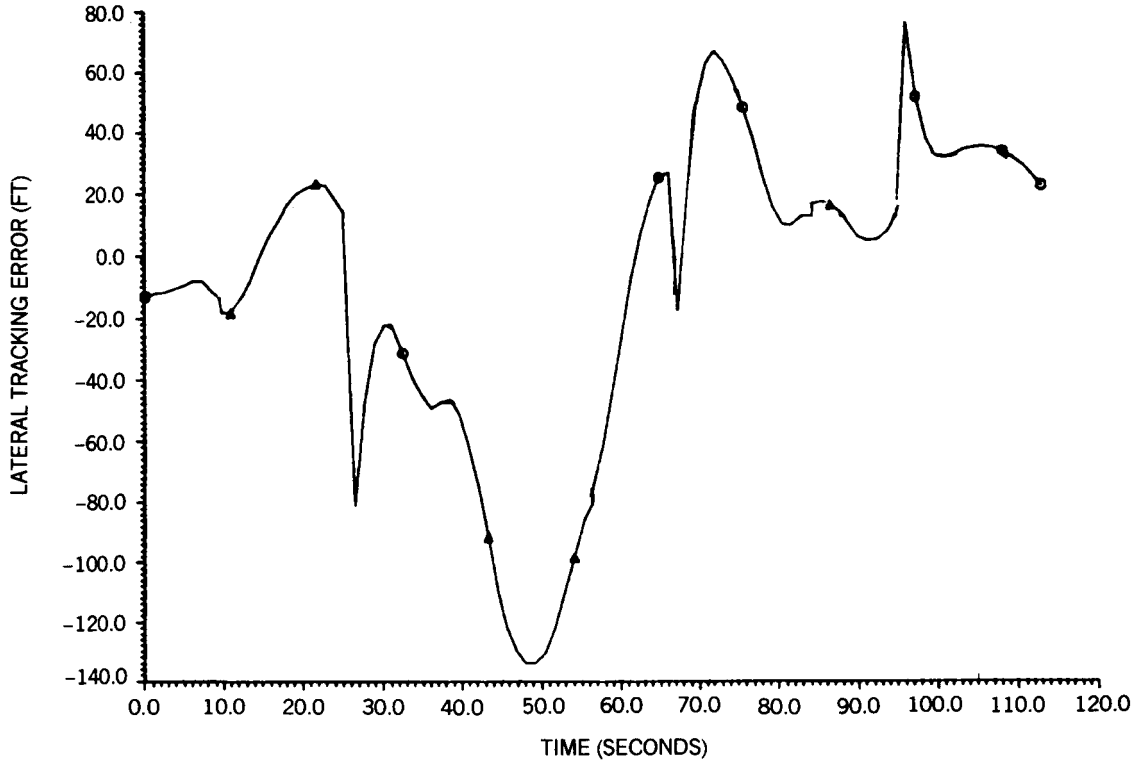

Figure 50. Lateral Tracking Error, Case 9 (Final Approach, Wind Shear)

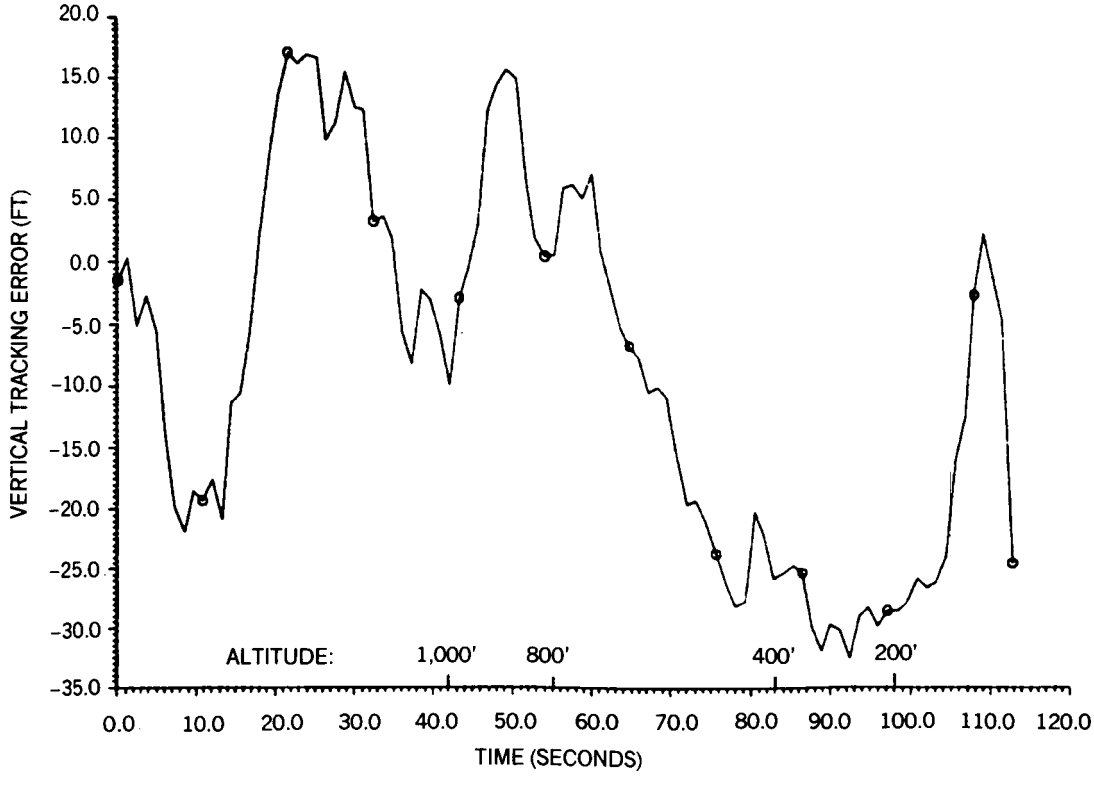

Figure 51. Vertical Tracking Error, Case 9 (Final Approach, Wind Shear)

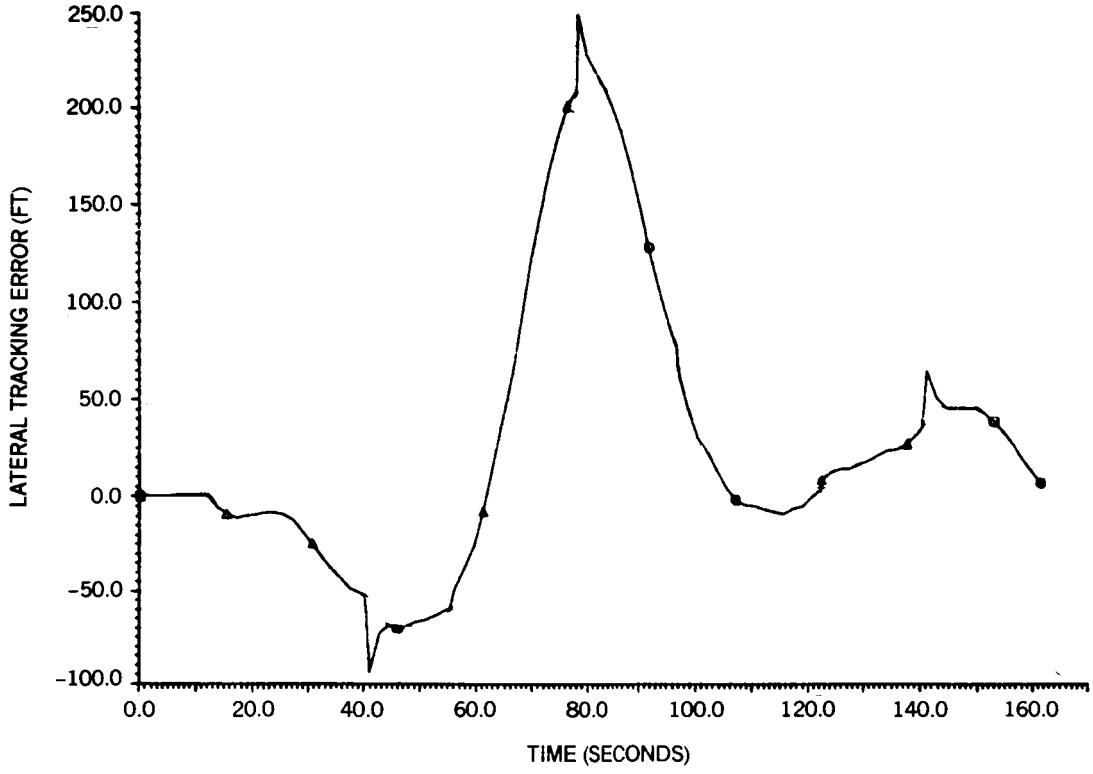

Figure 52. Lateral Tracking Error, Case 10 (Final Approach, Light Weight)

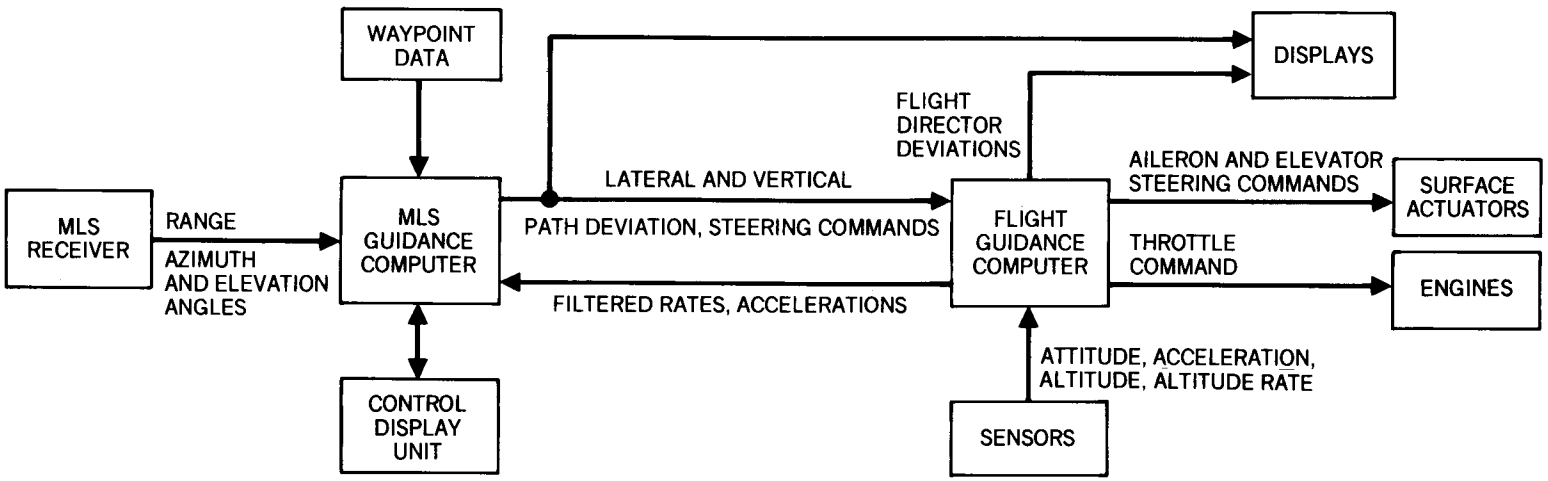

Figure 53. Interface Between MLS Guidance Computer and Existing Aircraft Systems

Standard Bibliographic Page

1. Report No. NASA CR-178182	2. Government Accession No.	3. Recipient's Catalog No.
4. Title and Subtitle GUIDANCE LAW SIMULATION STUDIES FOR COMPLEX APPROACHES USING THE MICROWAVE LANDING SYSTEM (MLS)		5. Report Date NOVEMBER, 1986
		6. Performing Organization Code
7. Author(s) J. B. FEATHER		8. Performing Organization Report No.
9. Performing Organization Name and Address DOUGLAS AIRCRAFT COMPANY 3855 LAKEWOOD BLVD. LONG BEACH, CA. 90846		10. Work Unit No.
		11. Contract or Grant No. NAS1-18028
12. Sponsoring Agency Name and Address NATIONAL AERONAUTICS AND SPACE ADMINISTRATION WASHINGTON DC 20546		13. Type of Report and Period Covered CONTRACTOR REPORT
		14. Sponsoring Agency Code 505-45-33-56

15. Supplementary Notes

LANGLEY TECHNICAL MONITOR: C. R. SPITZER
FAA TECHNICAL MONITOR: W. F. WHITE

16. Abstract

This report documents results for MLS guidance algorithm development conducted by DAC for NASA under the Advance Transport Operating Systems (ATOPS) Technology Studies program (NAS1-18028). The study consisted of evaluating guidance laws for vertical and lateral path control, as well as speed control, by simulating an MLS approach for the Washington National Airport. This work is an extension and generalization of a previous ATOPS contract (NAS1-16202) completed by DAC in 1985. The Washington river approach was simulated by six waypoints and one glideslope change and consisted of an eleven nautical mile approach path. Tracking performance was generated for 10 cases representing several different conditions, which included MLS noise, steady wind, turbulence, and windshear.

Results of this simulation phase are suitable for use in future fixed-base simlator evaluations employing actual hardware (autopilot and a performance management system), as well as crew procedures and information requirements for MLS.

17. Key Words (Suggested by Authors(s)) MICROWAVE LANDING SYSTEM (MLS) TERMINAL AREA GUIDANCE CURVED APPROACHES	18. Distribution Statement UNCLASSIFIED - UNLIMITED

19. Security Classif.(of this report) UNCLASSIFIED	20. Security Classif.(of this page) UNCLASSIFIED	21. No. of Pages 80	22. Price

For sale by the National Technical Information Service, Springfield, Virginia 22161

NASA Langley Form 63 (June 1985)